

A COMPREHENSIVE REVIEW OF GRAPHENE NANOPATELETS FOR REMOVAL AND DETECTION OF HEAVY METALS AND ENDOCRINE DISRUPTING COMPOUNDS

(Satu Komprehensif Kajian Semula Berkenaan Nanoplatelet Grafin untuk Penyingkiran dan Pengesanan Logam Berat dan Sebatian yang Mengganggu Endokrin)

Sazlinda Kamaruzaman^{1, 2*}, Najihah Mohammad Nasir¹, Yugarani Arivalagan¹, Noorfatimah Yahaya³, Saw Hong Loh⁴, Nor Suhaila Mohamad Hanapi⁵, Wan Nazihah Wan Ibrahim⁵ and Ili Syazana Johari¹

¹Department of Chemistry, Faculty of Science, Universiti Putra Malaysia, Serdang 43400, Selangor, Malaysia

²Natural Medicines and Product Research Laboratory (NaturMeds), Institute of Bioscience (IBS), Universiti Putra Malaysia, 43400, UPM Serdang Selangor, Malaysia

³Department of Toxicology, Advanced Medical and Dental Institute (AMDI), Universiti Sains Malaysia, 13200 Bertam Kepala Batas, Penang, Malaysia

⁴Faculty of Sciences and Marine Environment, Universiti Malaysia Terengganu, 21030 Kuala Nerus, Terengganu, Malaysia

⁵Faculty of Applied Sciences, Universiti Teknologi MARA, Shah Alam 40450, Selangor, Malaysia

*Corresponding author: sazlinda@upm.edu.my

Received: 29 August 2023; Accepted: 3 October 2023; Published: 29 December 2023

Abstract

Heavy metals and endocrine disrupting chemicals (EDC) have disruptive effects on an intact organism or its progeny. Due to the widespread presence of heavy metals and EDC in waterways, it is important to determine how effectively these compounds are removed from the environment. Their concentration has attained dangerous levels because of numerous anthropogenic activities such as industrial operations, particularly mining, agricultural processes, and the disposal of industrial waste materials. Heavy metals and EDC have been removed using a variety of effective approaches, including chemical oxidation, biodegradation, liquid extraction, membrane techniques, chemical precipitation, ion exchange, reverse osmosis, coagulation, flocculation, etc. These methods have several drawbacks, including a high reagent requirement, unpredictable metal ion removal, the generation of toxic sludge, etc. Adsorption is a method that shows promise because of its simple design, low cost, and high efficiency. Its ability to remove hazardous and micropollutants from wastewater is what makes it the method of choice. The use of graphene nanoplatelets (GNPs) as adsorbents in the treatment of water has been established by research. A wide range of water pollutants, including but not limited to organic molecules and inorganic heavy metals, are reported to be effectively remedied by GNPs. The high surface areas and modifiable functional groups of GNPs can be used to remove various contaminants in water and wastewater treatment processes. More significantly, because GNPs are mainly made up of carbon, this characteristic makes it easier to use these carbon-based materials for adsorbing pollutants in water and wastewater treatment systems. In the present review, the mechanisms of adsorption are demonstrated by investigating the kinetics, isotherms, and thermodynamics of adsorption. Besides that, pH, contact

time, adsorbent dosage, and initial analyte concentration were investigated.

Keywords: graphene nanoplatelets, endocrine disrupting compounds, heavy metals, isotherm, kinetics, thermodynamic

Abstrak

Logam berat dan bahan kimia pengganggu endokrin (EDC) mempunyai kesan yang mengganggu pada organisma yang utuh atau keturunannya. Disebabkan kehadiran meluas logam berat dan EDC dalam laluan air, adalah penting untuk menentukan keberkesanan sebatian ini dikeluarkan dari alam sekitar. Kepekatan mereka telah mencapai tahap berbahaya kerana banyak aktiviti antropogenik seperti operasi perindustrian, terutamanya perlombongan, proses pertanian, dan pelupusan bahan buangan industri. Logam berat dan EDC telah dialih keluar menggunakan pelbagai pendekatan yang berkesan, termasuk pengoksidaan kimia, biodegradasi, pengekstrakan cecair, teknik membran, pemendakan kimia, pertukaran ion, osmosis songsang, pembekuan, pemberbukan, dll. Kaedah ini mempunyai beberapa kelemahan, termasuk yang tinggi. keperluan reagen, penyingkiran ion logam yang tidak dapat diramalkan, penjanaan enap cemar toksik, dsb. Penjerapan ialah kaedah yang menjanjikan kerana reka bentuknya yang ringkas, kos rendah dan kecekapan tinggi. Keupayaannya untuk membuang bahan pencemar berbahaya dan mikro daripada air sisa adalah yang menjadikannya kaedah pilihan. Penggunaan graphene nanoplatelets (GNPs) sebagai penjerap dalam rawatan air telah ditubuhkan oleh penyelidikan. Pelbagai bahan pencemar air, termasuk tetapi tidak terhad kepada molekul organik dan logam berat bukan organik, dilaporkan akan dipulihkan dengan berkesan oleh KNK. Kawasan permukaan yang tinggi dan kumpulan fungsi GNP yang boleh diubah suai boleh digunakan untuk membuang pelbagai bahan cemar dalam air dan proses rawatan air sisa. Lebih ketara, kerana KNK kebanyakannya terdiri daripada karbon, ciri ini memudahkan penggunaan bahan berasaskan karbon ini untuk menjerap bahan pencemar dalam sistem rawatan air dan air sisa. Dalam kajian ini, mekanisme penjerapan ditunjukkan dengan menyiasat kinetik, isoterma, dan termodinamik penjerapan. Selain itu, pH, masa sentuhan, dos penjerap, dan kepekatan analit awal telah disiasat.

Kata kunci: kepingan nano grafit, sebatian mengendala endokrin, logam berat, isoterma, kinetik, termodinamik

Introduction

Heavy metals are one of the environmental contaminants present in water [1]. In this era, heavy metals have emerged as life-threatening pollutants if left untreated. Heavy metals are one of pollutant that has been thoroughly studied in the research that have worked on the development of graphene applications in the sectors of water and wastewater treatment technologies. Heavy metals include lead, arsenic, cadmium, cobalt, copper, gold, palladium, and zinc, among others. Heavy metals are known for its toxicity and carcinogenicity to human beings. Long term exposure to heavy metals can cause a detrimental to human body. Along with unlimited discharge of wastewater effluents, pollution of heavy metal has become a worldwide concern, which poses a potential threat to human and animals. For instance, lead ion (Pb^{2+}) exists widely in the wastewater, and it could enter human body with food or water, once excessive intake of them for a period, probably leads to some diseases including convulsions, renal failure, even cancer. Besides that, heavy metal ions have non-biodegradable properties which can cause severe health problems in

animals and human beings.

Endocrine disrupting chemicals (EDC) are external drug or mixture that may interfere with or modify the functions of the endocrine system, resulting in undesirable health effects in an organism, its offspring, or (sub) populations [2]. The substance may interfere with the synthesis, secretion, transport, binding, action, or elimination of natural hormones in the body, which are responsible for the maintenance of homeostasis, reproduction, development, and/or behaviour, as well as the regulation of developmental processes [3-5]. These two pollutants tend to harm the lives of living organisms, thus a lot of materials have been developed and their effectiveness in the removal of heavy metals is being studied. Nanotechnology is presently reclaiming a significant amount of effort due to their high surface area, small particle size, tremendous potential, excellent inherent reactivity, and capacities as a catalytic reagent of a pollutant through modifying reaction mechanisms. Therefore, due to their high efficacy in a wide range of contaminants – including organic compounds, inorganic compounds, pharmaceutical compounds, chlorinated

compounds, and nitro-groups – nanomaterials have been widely used in environmental applications. These nanomaterials for pollutant removal showed an effective wastewater treatment system under small-scale production; it is anticipated to be less expensive compared to other more traditional methods of removal [1].

Graphene has gained attention as a nanomaterial. Recent studies have been concentrating on the removal of various water pollutants using graphene in its pristine, functionalized, or composite forms [6], due to its flexibility in introducing functional groups and to its easy operation [7-9]. Graphene is composed of carbon atoms organized in a 2D hexagonal array, which gives graphene its characteristic honeycomb structure. Every carbon atom creates three covalent bonds with its closest neighbour as a result of the sp^2 hybridized orbitals being coplanar and aligned at 120° to one another, while the remaining $2p_z$ orbital forms a bond with an electron density that is above and below the basal plane. The exceptional electrical and thermal properties of monolayer, bilayer, and few-layer graphene are brought about by the aromatic electron cloud and honeycomb crystal lattice [10]. According to Stoller et al., graphene is suited for adsorption due to its high porosity and exceptional specific surface area of $2600 \text{ m}^2.\text{g}^{-1}$ [11]. Graphene layer, turbostratic carbon, bilayer graphene, trilayer graphene, multi-layer graphene (MLG), few-layer graphene (FLG), exfoliated graphite (EG), graphene oxide (GO), and reduced graphene oxide (rGO) are all well-known graphene-based materials. This combination of excellent properties has made graphene-based material a promising material for a wide range of applications, such as biological engineering, drug delivery, biosensor [12], biological agents [13], tissue engineering [14], and contaminant sensing [15].

Due to the difficulty and complexity of graphene fabrication, graphene nanoplatelets (GNPs) are also being extensively explored. GNPs are more approachable, have similar characteristics, and can be utilized for the same applications as graphene [16]. GNPs in one of the graphene derivatives consisted of a single to a few layers of sp^2 -bonded carbon atoms that

interacted to generate nanometre-sized two-dimensional particles. GNPs are composed of single and few layer graphene mixed with thicker graphite; hence, structurally they are in between graphene and graphite [17]. GNPs with a typical thickness of 5–10 nanometres are available in diameters as large as 50 microns. GNPs are cheaper and simpler to create than single-layered graphene and carbon nanotubes, making their utilization appealing [18]. These fascinating nanoparticles consist of 10–30 platelet-shaped graphene sheets identical to those seen in the walls of carbon nanotubes, but in a planar form retaining the single-layer characteristics [19]. Due to their platelet structure, they have a surface area per unit mass that is significantly larger than that of graphite and carbon nanotubes [20]. Considering all these characteristics, GNPs are valuable in numerous domains of research. It can be utilized as a novel and effective analytical adsorbent material [21]. Due to the direct exfoliation of affordable graphite flakes, e.g. by ultrasonics in acid baths, followed by chemical oxidation and reduction of graphite oxide nanoplatelets, GNPs are currently regarded as one of the most remarkable materials [22]. GNPs has recently attracted significant interest as a new and ideal material for the detection of environmental pollution involving water treatment [23], heavy metal ion detection [24], and green technology. Graphene is hydrophobic; therefore, stable dispersions in polar liquids can only be achieved by using the appropriate surfactants [17]. Figure 1 summarizes the chemical properties of graphene-based materials.

The aspect ratios of GNPs can range into the thousands. They exhibit the same thermal and mechanical properties as carbon nanotubes but have greater surface areas or aspect ratios. Considering this, GNPs can be used to improve the properties of a wide range of polymeric materials, including thermoplastic and thermoset composites, natural or synthetic rubber, thermoplastic elastomers, adhesives, paints, and coatings. The GNPs are offered in a granular form that in water, organic solvents and polymers with the right choice of dispersion aids, equipment and techniques [25].

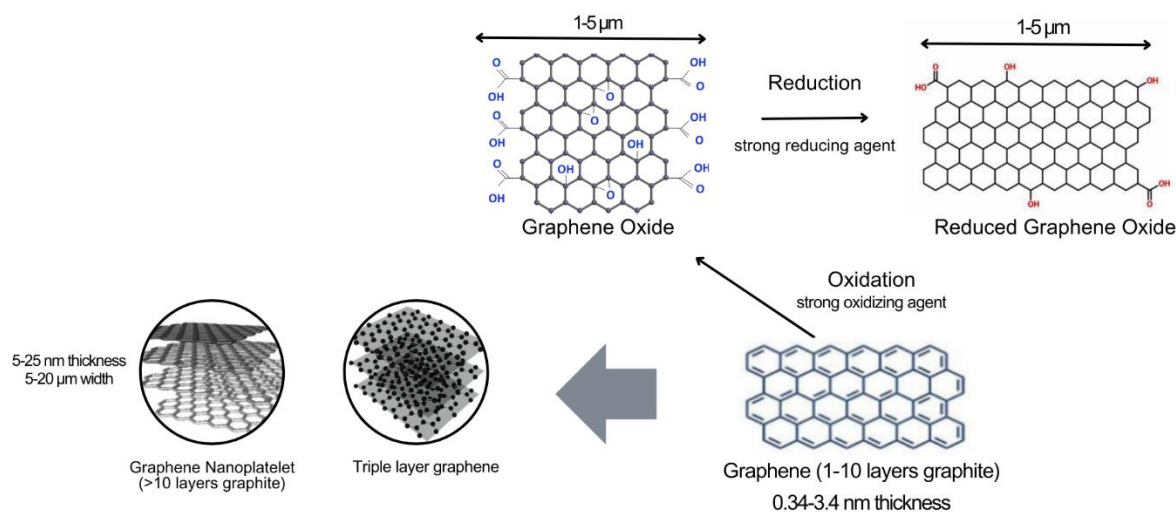


Figure 1. The chemical properties of graphene-based materials

An et al. conducted research on two types of graphene flakes manufactured by the non-oxidative and oxidative routes. In this work, their morphology, crystallographic order, gas adsorption potential, and electrical conductivity were examined [26]. The morphological differences of graphene nanoplatelets produced by oxidative (rGO-NP) and nonoxidative (GIC-NP) processes were compared using several analytical techniques. The adsorptive potential peaks of rGO-NP were found to be significantly more dispersed over the basal and non-basal regions than those of GIC-NP, indicating a heterogeneous surface. Comparing the Raman spectra and transmission electron microscope (TEM) pictures of the rGO-NP and GIC-NP, distinct crystallographic flaws were discovered in the rGO-NP. Compared to the GIC-NP, the R-ratio values evaluated at the edge and basal plane of the rGO-NP were substantially similar. Based on the overall analytical results and characteristics demonstrated in this comparative study, it is believed that GIC-NP is a more advantageous material than rGO-NP for numerous applications, such as conductive inks and conductive additives for batteries, where electric conducting properties are crucial. Consequently, the degree of disagreement in the R-values between the edge and basal plane can be employed as a significant criterion in the quality control of graphite nanoplatelets produced via diverse ways [26].

Exfoliated graphite nanoplatelets (xGnP) are a novel

efficient adsorbent material with high adsorption capacity, good stability, and rapid adsorption, with platelet thicknesses in the nanometre range but platelet areas in the micrometre range [27, 28]. In addition, xGnP may be easily extracted from inexpensive, natural graphite in huge quantities, without the requirement for dimension expansion, for water purification applications. These materials are cheaper than carbon nanotubes, can be included into water treatment procedures, and are simple to remove or renew [29].

GNPs exhibit its large surface area, accessible surface, high hydrophobicity, and high mechanical properties, enabling it to be explored and used widely in the removal of heavy metals and EDCs. Moreover, enormous, delocalized π - π electron system that GNPs owe enables the formation of strong bonding with heavy metals and EDCs [30], making the removal process efficient. This article provides a general overview of GNPs being used for the removal of heavy metals. Adsorptive removal of heavy metals is discussed by studying the kinetics, isotherms, and thermodynamics of adsorption. Adsorption parameters which include pH, are also investigated.

Graphene nanoplatelets as adsorbents for the removal of heavy metal ions

According to Briffa et al. [31], heavy metals are defined as naturally occurring elements with high atomic weights and densities greater than 5 g/cm³ that are

characterised by high stability but low levels of biodegradability, which cause bioaccumulation and biomagnification in living things. According to their toxicological characteristics, heavy metals can either be essential or non-essential for enzymatic activity [32]. The first is crucial for living things and can be present in little amounts; it only becomes harmful at a particular concentration threshold. Disease or abnormalities are caused by an essential heavy metal's excess or deficiency. The most hazardous substances, on the other hand, are non-essential heavy metals since they are difficult to break down through biological and photochemical processes and have harmful effects on both plants and animals, including people. According to Sall et al. [33], heavy metals have a number of negative health impacts, including impaired growth and development, cancer, organ damage, and, in larger amounts, death.

Heavy metals are one of the pollutants that has been thoroughly studied in the development of graphene applications in the sectors of water and wastewater treatment technologies. Heavy metals include lead, arsenic, cadmium, cobalt, copper, gold, palladium, and zinc, among others. Heavy metals have piqued the interest of researchers who are interested in finding a solution to this problem, which can have detrimental impacts on human health and the environment. Bioreactors [34], degradation and photodegradation [35-38], filtration [39], photocatalysis [40, 41], photo-Fenton and Fenton-like [42, 43], coagulation [44] and adsorption [45, 46] are all utilized to remove contaminants from water. Among these technologies, adsorption is the most popular and effective method for treating wastewater. This methodology is superior and considered powerful alternatives to conventional methods [47] because of its low cost, ease of operation, high efficiency, high capacity, simplicity, dependability, and low energy usage [48, 49]. Due to its large specific surface area, delocalized π -electron system, which can form strong interactions with other which is perfect for adsorption, GNP are utilized as an adsorbent to remove the contaminants [30].

The research by Kucherovala et al. [50] focused on the adsorption of Pb(II) ions onto graphene materials

prepared through the exfoliation of a hydrolysed extended graphite intercalation compound. Few-layered oxidized graphene suspension (FLOGS), multi-layered graphene paste (MLGP), and few-layered graphene paste (FLGP) were employed as adsorbents for the removal of Pb(II) from aqueous solutions. These adsorbents were reported to have maximum experimental Pb(II) adsorption capabilities of 850, 230, and 170 mg/g, respectively. To fit the experimental data, two adsorption isotherm models were applied: Langmuir and Freundlich. The Langmuir model assumes that adsorption occurs at specific homogeneous sites on the adsorbent surface. For non-ideal sorption onto heterogeneous surfaces with multiple layers, the Freundlich model is reported to be more fit. The Type III S-shaped isotherms observed for FLOGS suggest a transitional porous structure of the adsorbent with a complex pore space topology and a wide range of pore sizes. Additionally, the nature of that isotherm's steepness shows that the adsorbent has mostly very small pores. From the origin to the inflection point, the lower portion of the S-shaped curve corresponds to the creation of a monomolecular layer, and the subsequent rise of the curve is explained by the transition from mono- to multi-molecular adsorption. It can be assumed that the adsorption isotherms created for the FLGP and MLGP correspond to L-type curves.

Using functionalized graphite nanoplatelets (FGN) based electrodes, Mishra et al. [51] demonstrated the simultaneous removal of sodium and both pentavalent and trivalent forms of arsenic from an aqueous solution. Furthermore, these electrode-based water filters were employed to extract various metals from seawater. The preparation of graphite nanoplatelets (GNP) involved acid intercalation followed by thermal exfoliation, with additional acid treatment to functionalize the GNP. The performance of a supercapacitor-based water filter was evaluated for removing high concentrations of trivalent and pentavalent arsenic, sodium, and for desalinating seawater, using cyclic voltammetry (CV) and inductively coupled plasma-optical emission spectroscopy (ICP-OES) techniques. The transient behaviour of the metal adsorption process was analysed using the Elovich and intra-particle diffusion kinetic models. Solutions containing sodium arsenate and

sodium arsenite with an initial arsenic concentration of 300 ppm were employed to study the concurrent transient behaviour of sodium and arsenic adsorption. Both the Elovich and intra-particle diffusion kinetic models provided comparable fits for the metallic impurities. The Elovich model pertains to diffusion, while the intra-particle diffusion kinetic model is derived from chemical reaction kinetics. The removal efficiency of the supercapacitor-based water filter was investigated for salt removal, both forms of arsenic, and desalination of seawater. Approximately 72% of arsenic (As) and 75% of sodium (Na) removal efficiency was achieved for sodium arsenate-containing water, while for sodium arsenite-containing water, the removal efficiency was determined to be 73% for arsenic and 76% for sodium. These results were obtained over 20 repeated cycles with 100 mg of FGN loading on each electrode.

Ion et al. [28] conducted an investigation into the sorption behaviour of Pb(II) onto exfoliated graphite nanoplatelets (xGNPs). Among various factors such as specific surface area and solution composition, the presence of surface functional groups emerges as the paramount determinant influencing Pb(II) adsorption on xGNPs. Nitric acid (HNO₃) oxidation plays a crucial role in modifying the ion-exchange capacity, leading to the development of distinct acidic functional groups on the surface, which exhibit dissociation at varying pH levels. Due to the surface functionalization by HNO₃ and additional oxygen-containing groups like hydroxyl, carbonyl, and carboxyl, the adsorption capability of xGNPs treated with concentrated HNO₃ exhibit a substantially enhanced capacity of 13.09 mg/g. The sorption characteristics are profoundly impacted by pH, the presence of active sites and the surface dimensions. The influence of pH was revealing that adsorption percentages reach 100% at pH 6, but rapidly decreased at more acidic pH values. At low pH levels, lead is present as free cations, which is explained by the fact that at these pH levels, the H⁺ concentration is large, and protons can compete with lead ions for surface sites. The deprotonation of the sorbent functional groups causes a decrease in positive surface charge as pH rises. The sorption properties of the adsorbent in water were described using the Langmuir and Freundlich isotherm

models. Both models displayed excellent agreement with experimental data, as evidenced by correlation coefficient values of 0.9996 and 0.994 for Langmuir and Freundlich, respectively with the optimum initial concentration of 200 ppm at 30 min.

Sheng et al. also conducted an investigation into functionalized graphene nanoplatelets (FGN) by the acidic treatment of graphene nanoplatelets (GNPs) with HNO₃ for removing Pb(II) from solution. Through nitrogen desorption isotherm analysis, BET data revealed FGN's surface area is 714.5 m²/g, with an average pore size of 4.8502 nm and a pore volume of 0.8598 cm³/g. These findings indicate FGN's uniform and mesoporous nature. The specific surface area and effective adsorption sites of FGN facilitated Pb(II) adsorption at lower initial concentrations. However, as the initial Pb (II) concentration increased, the percentage removal was decreased due to the electrostatic repulsion among heavy metal ions and increased competition between heavy metal ions for adsorption sites. This study also stated that the capacity for Pb(II) adsorption notably increased as pH shifted from 6 to 7, resulting in approximately 100% removal efficiency of Pb(II) by FGN at pH 7 due to precipitation and adsorption coefficients. The dominant role of monolayer chemical adsorption on FGN's surface was reported while the pseudo-second order kinetic model achieved an R² of 0.998, indicating a better fit for the latter. This suggests that valence forces, involving electron exchange or sharing between FGN and Pb(II), may govern the rate-limiting step in the adsorption process [52].

Nandi et al. conducted research on GNPs obtained from human nails and synthesized via a novel *in-situ* synthetic technique involving ferric chloride. This work suggests that the surface of GNPs is mostly positively charged pH < 6 and predominantly negatively charged pH > 6. The highest sorption capacity was reported at pH = 7.0 since the surface of GNPs is almost neutral. However, the sorption capacity of GNPs towards As (III) is decreased at lower or higher pH values than pH = 7.0. The sorption of As(III) on the surface of GNPs happens at pH 7.0 via ion-dipole interaction. The sorption of As(III) fitted the Langmuir model (R² = 0.97) can be attributed to the GNPs' high specific surface area and more accessible

opening sites at lower adsorbate concentrations. Notably, the pseudo-second order model provided the best agreement with the experimental data. In addition, thermodynamic analysis offered insight into the reaction's feasibility, nature, and direction. The negative value of ΔG^0 indicated the spontaneous nature of the As(III) adsorption process on GNPs with respect to temperature changes. The positive ΔH^0 value indicated an endothermic reaction, while the increase in entropy ΔS^0 suggested greater randomness at the solid-liquid interface [53].

Zhu et al. have developed magnetic graphene nanoplatelet composites (MGNCs) by synthesizing core-shell Fe-Fe₂O₃ nanoparticles (NPs) through a straightforward one-pot thermal decomposition process. According to this study, MGNCs, comprising GNPs decorated with NPs, showed robust magnetization for magnetic separation and efficiently adsorb arsenic(III) from polluted water. This is due to the magnetic graphene nanoplatelets increasing the adsorption sites. Other than that, the solution pH dominantly affects the surface charge of the adsorbent, and the optimum adsorption capacity of 11.34 mg/g was achieved when the sample solution is at pH 7. Langmuir and Freundlich models fit well ($R^2 > 0.95$), revealing a specific homogenous adsorption mechanism. MGNC's greater surface area (42.1 m²/g) enhances adsorption capacity. Favourable adsorption is shown by Freundlich parameter ($n = 2.79 > 1$) and fitted with pseudo-second order kinetics ($R^2 = 0.994$) and describe the As (III) removal with the chemisorption process [54].

Samaraweera et al. studied the significance of the adsorption method, particularly when dealing with pollutant removal, such as Cu²⁺ ions. In their research, they investigated the potential of using a hybrid material consisting of graphene and pine wood biochar (GPBC) as an adsorbent for Cu²⁺ ions. The study found that biochar, when functionalized with nanomaterials like graphene, can greatly enhance its ability to remove pollutants. This enhancement occurs when both the nanomaterial and the biochar surface act as effective adsorption sites for the target pollutants. Interestingly, the researchers used different types of graphene nanosheets (GNPs) with varying surface areas (G1, G2,

and G3) to create GPBCs. They noted that GPBCs with lower surface areas were produced using GNPs with larger surface areas. This counterintuitive observation was attributed to potential pore-filling and pore-blocking effects of the nanomaterials within the biochar. The study focused on GPBC-1, which had the lowest nanophase surface area but the highest Cu²⁺ ion adsorption capacity. This finding challenges the conventional belief that higher surface area always leads to better adsorption. In the case of GPBC-1, Cu²⁺ removal occurred through electrostatic interactions, inner sphere surface complex formation, and other attractive forces with oxygenated functional groups on the GPBC-1 surface. The researchers employed Langmuir and Freundlich isotherm models to understand the interaction between the adsorbate (Cu²⁺) and the adsorbent (GPBC-1). The Langmuir model, which assumes monolayer adsorption, provided a better fit to the data. Additionally, kinetic models revealed that the adsorption process followed pseudo-second order kinetics, indicating a strong interaction between Cu²⁺ ions and GPBC-1. Thermodynamic studies also showed that Cu²⁺ sorption on GPBC-1 was an endothermic process, requiring energy input. The negative values of ΔG at various temperatures indicated that the adsorption was spontaneous. Positive ΔS^0 values suggested an increase in randomness during the adsorption process, controlled by entropy [55].

Rosenzweig et al. investigated Cu²⁺ ion adsorption on various nanomaterials, including carbon nanotubes and different types of graphene nanoparticles (GNPs). They found that functionalized GNPs, such as GNP-COOH and GNP-O⁺, exhibited better stability in water, a crucial factor for effective pollutant removal. The study applied these optimized conditions to Cu²⁺ adsorption experiments using GNPs. The adsorption behaviour was analysed using the Freundlich model, revealing that GNPs with 1/n values significantly > 1 had weaker adsorption power, likely due to the formation of irreversible aggregates caused by strong van der Waals forces within multilayer nano-sheets. These aggregates could reduce the adsorption capacity of GNPs by concealing adsorption sites. However, functionalized GNPs maintained high colloidal stability, thanks to oxygen-containing groups at their edges, preventing

excessive aggregation and ensuring a larger accessible surface area for adsorption. This study highlights the importance of nanomaterial properties, especially colloidal stability, in Cu^{2+} ion adsorption, and underscores the impact of functionalization on the effectiveness of GNPs in water treatment applications [56].

Capra et al. examined the removal of Sb(III) from drinking water using oxidized exfoliated graphite nanoplatelets (ox-xGNP). They observed irregularly shaped Sb(III) particles ranging from 50 to 200 nm in TEM images. Notably, the adsorption capacity increased significantly, reaching 16.0 mg/g at a pH of 9.0, a phenomenon influenced by both the composition of metal ions in the solution and alterations in surface functional groups on the adsorbent. Zeta potential measurements confirmed the negative charge on the ox-xGNP surface, which contributed to optimal colloidal stability at pH 9.0 due to electrostatic attractions. Despite the typical drinking water pH range of 6.0 to 8.0, experiments were conducted at pH 7.0 in anticipation of future Sb (III) removal applications. The established optimal removal conditions included a pH of 7.0, 1.0 mg ox-xGNP per 100 mL solution, a temperature of 293 K, 1.0 mg L^{-1} Sb(III), and a 25-minute contact time. Kinetic analysis favoured the pseudo-first order model ($R^2 = 0.999$), which accurately estimated the adsorption capacity at equilibrium. Furthermore, the Langmuir adsorption isotherm model best described the process, indicating monolayer adsorption on homogeneous ox-xGNP surfaces, emphasizing the favourable Sb(III) adsorption. Thermodynamic analysis unveiled spontaneous and favourable adsorption, potential randomness at the solid-solution interface, and an exothermic process [57].

Smith et al. studied a method for removing Cu(II), Zn(II), and Pb(II) ions from water using single-wall carbon nanotube-graphene nanoplatelet (SWCNT-GNP) aerogels, with varying amounts of carbon nanomaterials (0.2 wt.% and 2.0 wt.%). They tested the pH of metal (II) ion solutions to confirm that metal ion removal was solely due to adsorption and not precipitation, which occurred only at $\text{pH} > 6.19$. The adsorption of Cu(II) onto the aerogel followed a pseudo-second order kinetic

model. Initially, there was a rapid adsorption phase for about 75 minutes, after which the adsorption capacity gradually increased, reaching equilibrium at approximately 105 minutes for the 2.0 wt.% aerogel and 90 minutes for the 0.2 wt.% aerogel. The initial rise was attributed to the open valence of Cu(II) ions interacting with the network, saturating the carbon nanomaterial (CNM) aerogel. The sponge-like structure of the aerogel provided more adsorption sites, increasing surface area. The adsorption behaviour for Cu(II) ions was generally similar to that of Zn(II) and Pb(II) ions. However, the uptake capacity for Pb(II) decreased considerably within 120 minutes. This decrease was because Pb(II) has a higher molecular weight and ionic radius compared to Cu(II) and Zn(II), making it more challenging to adsorb as many ions as possible due to the direct association between uptake capacity and these parameters. Interestingly, the equilibrium isotherms for all three metals displayed a largely linear behaviour, unlike the typical Langmuir or Freundlich-type models [58].

Ahmad et al. explored the efficacy of three different adsorbents, namely hybrid graphite nanoflakes/mesoporous silica nanoparticles (GNP-MSN), amine-functionalized mesoporous silica (NH_2 -MSN), and graphite nanoflakes (GNP), for the removal of lead from aqueous solutions. The surface area of GNP-MSN was reduced, likely due to the silica coating on GNP surfaces, and the pore size of GNP-MSN was slightly larger than that of GNP, influenced by the presence of ionic template C16PyBr. Furthermore, functionalizing MSNs with amine groups led to a decrease in surface area and pore volume, attributed to the integration of amine groups onto pore surfaces. The maximum lead(II) adsorption for all three adsorbents occurred at pH 4 within 20 minutes. Lower pH hindered adsorption due to hydronium ions surrounding GNP surfaces, obstructing lead(II) ion binding sites. At higher pH, metal cation precipitation occurred. Adsorption kinetics revealed that the pseudo-second order model was the most suitable for describing lead(II) ion adsorption on both GNP and NH_2 -MSN, suggesting chemisorption. The pseudo-first order and pseudo-second order models yielded lower R^2 values for GNP-MSN, indicating adsorption controlled by physical adsorption or chemical adsorption involving weak

intermolecular forces or strong surface complexation of metal ions with oxygen-containing groups. Langmuir and Freundlich adsorption isotherms were applied, with Langmuir better representing lead(II) ion adsorption by GNP and NH₂-MSN. This suggests monolayer coverage on their surfaces. Conversely, the Freundlich model indicated multilayer adsorption on GNP-MSN's surface, supporting the pseudo-second order kinetic model's suggestion of physisorption involving Van der Waals or dipole-dipole forces [30].

Bogdan et al. investigated the adsorption of ammonium ions from aqueous solutions using exfoliated graphite nanoplatelets (xGNP) as adsorbents. The study examined adsorption characteristics under different conditions, including contact times, initial ammonium ion concentrations, and temperatures. Optimal adsorption parameters were identified as 70 ppm ammonium ions at 25°C with 30 minutes of stirring. The adsorption mechanisms were analysed using pseudo-first order, pseudo-second order, and intra-particle diffusion models. Among these, the pseudo-second order model ($R^2 = 0.9831$) provided the best fit for describing the adsorption kinetics of ammonium ions onto xGNP. To explain how solutes interacted with the nanostructured carbon-based adsorbents at equilibrium; various isotherm models including Freundlich, Langmuir, Temkin, Halsey, and Harkins-Jura were applied. The data showed that equilibrium data fit well with Freundlich, Langmuir, Harkins-Jura, and Halsey adsorption isotherm models, indicating advantageous, multilayer adsorption, a heterogeneous surface, and pore distribution on xGNP. Thermodynamic parameters were also determined, revealing that the adsorption process was feasible due to the negative value of ΔG^0 . The positive value of ΔS^0 suggested ammonium molecules agglomerated at the solid/solution interface, and the endothermic nature of the adsorption process was indicated by the positive value of ΔH^0 [59].

Yin et al. conducted a study on the dispersive magnetic solid-phase extraction (MSPE) of copper and lead in *Panax notoginseng* using Fe₃O₄/graphene magnetic nanoparticles (Fe₃O₄@G) as adsorbents. They prepared Fe₃O₄/graphene magnetic nanoparticles by adding FeCl₃.6H₂O and (NH₄)₂Fe(SO₄)₂.6H₂O to dispersed

graphene nanoparticles. To develop a highly sensitive method for simultaneous determination of Cu(II) and Pb(II) in *Panax notoginseng*, they optimized various experimental conditions. The optimal sorbent dose for extracting Cu and Pb from samples was found to be 36 mg. pH played a critical role in the MSPE procedure, with the optimal pH at 7. The retention percentage of lead and copper ions on the sorbent decreased at pH values higher than 7, likely due to the precipitation of lead and copper ions in the hydroxide form, reducing the concentration of free ions. An equilibration time of approximately 12 minutes was required for quantitative extraction of the analytes from the solution into the solid phase. The method was validated by applying it to determine the content of Cu²⁺ and Pb²⁺ in *Panax notoginseng* using standard addition and recovery techniques. The results indicated spiked recoveries for the target metal ions in the range of 96.4% to 102.0%. Furthermore, the concentrations of the two ions were found to be very low in *Panax notoginseng* samples, demonstrating the effectiveness of the adsorbent in recovering copper and lead as described in the methods [60].

Kucherova et al. examined the adsorption of lead ions (Pb²⁺) using graphene-based nanocomposites derived from hydrolysed expanded graphite intercalation compound. Three distinct nanocomposites-suspension of graphene nanoplatelets (SGN), paste of multi-layered oxidized graphene (PMOG), and paste of few-layered oxidized graphene (PFOG)-were employed as adsorbents for Pb²⁺ extraction. The adsorption kinetics revealed an initial rapid Pb²⁺ adsorption rate that subsequently slowed, ultimately reaching equilibrium at 30 min. Remarkably, the adsorption capacities achieved were 457 mg/g (SGN), 103 mg/g (PMOG), and 38 mg/g (PFOG). The initial adsorption rate was influenced by the surface area energy of the adsorbents, resulting in a sudden increase in adsorption due to the presence of active adsorption sites. To discern the nature of the adsorption process (diffusion or chemisorption), various kinetic models, including the pseudo-first order, pseudo-second order, Elovich, and intraparticle diffusion models, were applied. Notably, the pseudo-second order model exhibited an excellent fit to the adsorption process, as evidenced by a high correlation coefficient

value ($R^2 = 0.999$) [50].

La et al. highlighted the potential of graphene nanoplatelets (GNPs) as a platform for even distribution of adsorbent nanoparticles to enhance electron exchange and ion transport for heavy-metal adsorption. They employed a thermal decomposition method to create a graphene-supported Fe-Mg oxide composite for efficient arsenic removal from aqueous solutions. The study investigated various factors affecting arsenic adsorption, including different Mg/Fe weight ratios, with initial As(V) concentrations at 10 ppm, an adsorbent dosage of 200 mg/L, pH 7, and room temperature. The addition of GNPs and Fe-Mg oxide significantly improved As(V) adsorption under these optimized conditions. Adsorption isotherms were used to assess arsenic adsorption and calculate the maximum As (V) adsorption capacity of the GNP/FeMg oxide composite. The Freundlich model provided a better fit (correlation coefficient of 0.985) compared to the Langmuir model (correlation coefficient of 0.935) for describing the adsorption behaviour of As(V) by the composite. Additionally, the kinetics of As(V) adsorption on the GNP/FeMg oxide surface were examined using the pseudo-second order model, showing a well-fitted correlation coefficient of 0.957. This suggests electron exchange occurred during the chemical adsorption process between the composite and arsenic. The selectivity of the GNP/FeMg binary oxide adsorbent for arsenic was tested in the presence of common metal ions typically found in drinking water, such as Na^+ , K^+ , Ca^{2+} , and Mg^{2+} . Notably, only a minimal amount of Na^+ , K^+ , and Ca^{2+} ions were adsorbed by the composite, whereas over 95% of arsenic

was effectively removed. Interestingly, the release of Mg from the adsorbent led to a 10% increase in the concentration of Mg^{2+} in the solution after adsorption [61].

Li et al. conducted research on the adsorption of Pb^{2+} and Cd^{2+} onto GNPs prepared through thermal exfoliation from water. The study investigated the influence of four key factors: pH, adsorption time, temperature, and initial concentration on the adsorption of Pb^{2+} and Cd^{2+} onto GNPs, ultimately determining the maximum adsorption capacities under optimized conditions. The results revealed that the adsorption percentages of Pb^{2+} and Cd^{2+} onto GNPs were 96.27% at pH 5.80 and 76.75% at pH 6.30, respectively. The adsorption process reached equilibrium rapidly, within just 30 minutes, indicating that GNPs have great potential as effective adsorbent materials. Furthermore, the adsorption capacity increased with higher equilibrium concentrations of metal ions, gradually reaching saturation. Notably, Pb^{2+} exhibited a more pronounced adsorption capacity increase with increasing equilibrium concentration compared to Cd^{2+} , suggesting that Pb^{2+} adsorbs more readily onto GNPs. The temperature-adsorption relationship indicated that the adsorption of metal ions onto GNPs is an exothermic reaction, with room temperature being favourable for the adsorption process. Additionally, the study highlighted the inverse relationship between pore size and uptake capacity, with GNPs exhibiting a high content of micro- and mesoporosity, making them excellent candidates for the removal of Pb^{2+} and Cd^{2+} ions [62].

Table 1. Summary of adsorption of heavy metals onto graphene nanoplatelets

Adsorbent	Heavy Metal Ions	Adsorption Conditions	Adsorption Isotherm Model	Adsorption Kinetics Model	Adsorption Thermodynamic	Adsorption Capacity (mg/g) / Removal Efficiency (%)	Additional Remarks	Ref.
Multi-layered graphene paste	Pb(II)	CT=10min, [A]=200-350mg/L	Langmuir and Freundlich	-	-	230	FLGP and MLGP correspond to L-type curves which typical for Type IV isotherms.	[50]
Functionalized graphene nanoplatelets	Pentavalent and trivalent forms of arsenic	CT=40min, AD=100mg [A]=300mg/L	Langmuir and Freundlich	Elovich model (diffusion) Intra-particle diffusion (chemical reaction kinetics)		27mg/g for arsenate, 29mg/g for arsenite / 72%	The adsorption takes place at specific homogeneous sites located on the adsorbent surface.	[51]
Exfoliated graphene nanoplatelets	Pb(II)	CT=30min, pH=6.0, [A]=200mg/L	Langmuir and Freundlich	-	-	13.09	-	[28]
Functionalized graphene nanoplatelets	Pb(II)	CT=12h, pH=6.0, AD=50mg, [A]=30 mg/L	Langmuir	Pseudo-second order	-	57.77	Five cycles of repeated use.	[52]
Graphene nanoplatelets	As(III)	CT=3h, T=300K, pH=6.0, AD=25, [A]=5.0	Langmuir	Pseudo-second order	Endothermic, spontaneous process and reaction has occurred at the solid-liquid interface with increasing randomness	247.22mmol.kg ⁻¹	When the sample is at pH <7 the water molecules adsorb on GNPs surfaces more than As (III) species. At higher pH	[53]

Magnetic graphene nanoplatelets composites	As(III)	CT=60min, pH=7.0, [A]=20	Langmuir Freundlich	Pseudo-second order	-	11.34	values (>7.0), GNP's surfaces become predominately negative. These both phenomena lead to the less interaction of GNP with As (III). The larger deviation of the solution pH from the neutral state, the lower adsorption capacity is observed either in acidic or basic solutions. [54]
Graphene/pine wood biochar hybrid	Cu(II)	CT=24h, pH=6.0, AD=0.05g, [A]= 5mg/L, T=25 \pm 0.5°C	Langmuir	Pseudo-second order	Endothermic, spontaneous process and increase randomness	4.7 – 10.6	Uses of higher surface area GNP's produced the lower surface areas hybrid adsorbents. This is because biochar loaded with nanomaterials can have a pore filling and pore-blocking effect. [55]

GNP-COOH, GNP-P, GNP-O ⁺	Cu(II)	AD=0.1 g, [A]=0.53-0.59mg/L	Freundlich	-	-	16.7	Functionalized GNPs showed good colloidal stability which shows a good adsorbent in water because pollutants must have free and quick access to all adsorptive sites on the adsorbent surface.	[56]
Oxidized exfoliated graphite nanoplatelets (ox-xGnP)	Sb(III)	CT=25min, pH=7.0, AD=1.0mg, [A]=1.0mg/L, T=293K	Langmuir	Pseudo-first order	Exothermic, spontaneous process and increase in randomness	8.91	At range of pH 9.0, a significant increase in the adsorption capacity of Sb (III) on the ox-xGnP surface.	[57]
Single-wall carbon Nanotube-graphene nanoplatelet	Cu(II) Zn(II) Pb(II)	CT=100min, pH=6.1, [A]=0.1mg/L	Langmuir Freundlich	Pseudo-second order	-	-	Pb (II) lower in average uptake capacity compared to Cu (II) and Zn (II) due to larger molecular weight and ionic radius.	[58]
GNP-MSN GNP	Pb(II)	CT=2h, pH=4.0, AD=10mg, [A]=10mg/L	Langmuir	Pseudo-second order	-	23.94 1.11	At lower pH, adsorption was unfavourable due to the	[30]

Exfoliated graphite nanoplatelets	Ammonium	-	Freundlich, Langmuir, Harkins-Jura and Halsey	Pseudo-second order	Exothermic, feasibility process and increase in randomness	12.04	surface of the GNP could be surrounded by the hydronium ions (H_3O^+) that hinder lead (II) ions from reaching the binding site on the surface of the GNP.	[59]
Fe ₃ O ₄ /graphene magnetic nanoparticles	Cu(II) Pb(II)	CT=12min, pH=7.0, AD=36mg	-	-	-	96.4 102.2	Decrease in the percentage of lead and copper ions on the sorbent at pH values higher than 7 is due to precipitation of lead and copper ions in the hydroxide form which leads to decreasing the concentration of free lead and copper ions in the sample.	[60]

Suspension of graphene nanoplatelets (SGN)	Pb(II)	AD=0.01g, [A]=1,040mg/L	-	Pseudo-second order	-	457	Pb (II) adsorption is initially quite rapid. Then, the adsorption rate gets slower over time and reaches the constant value at 30 min	[63]
GNP/Fe-Mg oxide composite	As(V)	pH=7 AD=200mg/L, [A]=10 mg/L	Freundlich	Pseudo-second order		40.3	-	[61]
Graphene nanoplatelets	Pb(II) Cd(II)	CT=30min, pH=Pb ²⁺ 5.80; Cd ²⁺ 6.30, AD=15mg, [A]=500mg/L	-	-	-	460.20 72.39	The adsorption capacity increases with increasing equilibrium concentration of metal ions, and reaches saturation progressively.	[62]

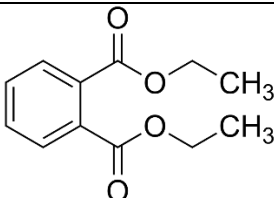
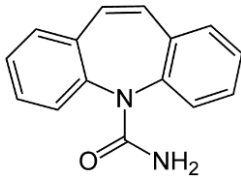
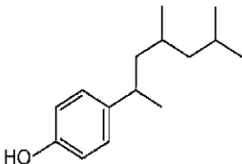
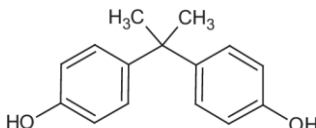
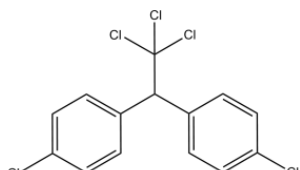
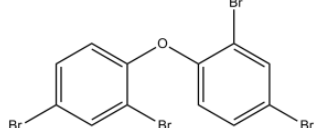
Abbreviations: FLOGS = few-layered oxidized graphene suspension; MLGP = multi-layered graphene paste; FLGP = few-layered graphene paste; FGN = functionalized graphite nanoplatelets; GNP-MSN = hybrid graphite nanoflakes/mesoporous silica nanoparticles; NH₂-MSN = amine functionalized mesoporous silica; GNP = graphite nanoflakes; SGN = suspension of graphene nanoplatelets; PMOG = paste of multi-layered oxidized graphene; PFOG = paste of few-layered oxidized graphene; CT = contact time [h], T = temperature [°C], AD = adsorbent dose [g/L], [IC] = initial concentration [mg/L]

Graphene nanoplatelets as endocrine disrupting chemicals adsorbents

Kumar et al. [64] highlighted growing concerns over the presence of endocrine-disrupting chemicals (EDCs) in aquatic water bodies, especially fresh water environments, and their potential disruptive effects on indigenous fauna. In the past few decades, environmental toxins have interfered with the endocrine systems of humans and animals, leading to deleterious effects, particularly in reproduction and the development of secondary sexual traits [29, 3]. An

endocrine disruptor is an external drug or mixture that may interfere with or modify the function(s) of the endocrine system, resulting in undesirable health effects in an intact organism, its offspring, or (sub)populations [2]. The substance may interfere with the synthesis, secretion, transport, binding, action, or elimination of natural hormones in the body, which are responsible for the maintenance of homeostasis, reproduction, development, and/or behaviour, as well as the regulation of developmental processes [3-5]. Table 2 below shows the several examples of EDCs.

Table 2: Some known EDCs molecular structure and their uses

Example EDCs	Category/Use	Molecular Structure	Molecular Weight (g/mol)
Diethyl phthalate	Personal care products		222.24
Carbamazepine	Pharmaceutical		236.269
Nonylphenols	Industrial surfactants		220.35
Bisphenol A	Food contact materials		228.29
Dichlorodiphenyltrichloroethane	Pesticides		354.48
Polybrominated diphenyl ethers	Brominated flame retardants		564.7

According to Ternes et al. [65] and Shi et al. [66] human and animal excretions as inactive polar conjugates such glucuronides and sulphates and their incomplete removal in sewage treatment plants were the main causes of the presence of EDCs in water bodies and sediments. The primary environmental source for these chemicals is the direct discharge of untreated sewage to surface waters. EDCs can also leach from septic tanks or landfills, infiltrate the ecosystem through surface runoff, or enter the water directly by direct discharge from treatment plants [67-73]. Therefore, this emerging class of pollutants need effective treatments. The best approach for removing contaminants is adsorption because no byproducts would be created and water and the adsorbent could both be recycled. As a result, researchers are constantly looking for novel adsorbents and trying to come up with new, effective removal techniques. GNPs are a brand-new, very effective adsorbent material that has a high capacity for adsorption, good stability, and quick adsorption. The platelet thickness is in the nanometer range, but the areas are in the micrometre range [28, 74]. In addition, GNPs may be easily produced in huge quantities from inexpensive natural graphite without the requirement for dimensional enlargement for use in water purification. These materials are less expensive than CNTs, can be used in water treatment procedures, and are simple to remove or regenerate, making them an excellent option for EDC adsorption [29].

Zaka et al. [75] analyzed the diclofenac sodium removal effectiveness of GNPs in water. To figure out the optimal parameters for DCS removal by GNPs, many factors were explored. The different parameters include contact time, adsorbent dosage, the initial concentration of DCS, pH and temperature. At 25°C temperature, 3.5 g/L dosage of GNPs, pH of 5, 5 ppm concentration of DCS, and contact time of 40 minutes, the maximum elimination of 99% was recorded. The interaction of adsorbents with ionizable contaminants has been found to be strongly influenced by electrostatic attractions or repulsions. Under acidic pH conditions, DCS functions as a neutral molecule and is more attracted to the graphene surface. The hydrophobic effects as well as the π - π electron-donor attractions play a significant role in the adsorption process for $\text{pH} < \text{pK}_a$ of DCS since

GNPs has a negative charge on the surface for pH values larger than 2.2. The removal effectiveness is shown to diminish at pH levels higher than 4.2 because DCS ionises to produce a negatively charged ion that is electrostatically attracted to the surface of GNPs. Adsorption isotherms were plotted for each model to gain a better knowledge of the adsorption process and insight into the relationships between adsorbent and adsorbate. The adsorption isotherms were obtained under optimal conditions. In addition, the interactions between molecules of adsorbate and adsorbent were investigated using three distinct isotherm models: Langmuir, Freundlich, and Temkin. The data were determined to be best suited by the Langmuir isotherm, which had an R^2 value of 0.9967. The Langmuir isotherm model assumes that there are no lateral interactions between adsorbate molecules on the surface during monolayer adsorption. To comprehend the kinetics of DCS adsorption on GNPs, pseudo-first order and pseudo-second order kinetic models were utilised. With a rate constant of $K_2 = 1.8218 \text{ g/mg min}$, it was discovered that the adsorption process followed pseudo-second-order kinetics. The process was confirmed to be exothermic and spontaneous when the thermodynamic properties were computed using Sip's model and indicated the negative value of change in Gibbs free energy and the change in enthalpy was equal to -3.9089 KJ/mol.

Radu et al. [29] utilized exfoliated graphite nanoplatelets (xGnP) as adsorbents for bisphenol A (BPA). This research investigates the possibility of eradicating this endocrine disruptor. The influence of the following parameters on the sorption behaviour of xGnP was investigated: contact time, starting BPA concentration, temperature, ionic strength, and pH. The influence of solution pH on BPA removal was examined. It was found that BPA adsorption decreased when the pH value is below 4, likely as a result of protonation of the xGnP surface's negative charge. The deprotonation of BPA causes a decrease in the hydrophobic interactions between the electrons of the graphite surface and the electrons of the C=C double bonds of BPA above a pH value of 10, and as a result, the adsorption of BPA on the xGnP surface. Between pH 3 and 7, it was seen that BPA adsorption marginally

increased, and between pH 7 and 9, it started to decline. Based on research, the ideal circumstances were (0.1 mg of xGnP and 50 mL of 1-10 mg/L BPA at 298.15 K, pH = 5.5, and contact period 30 minutes). It was also investigated how the ionic strength of the working solutions affected the elimination of organic contaminants. Salts and organic materials from the environment increase the adsorption of BPA on xGnP surfaces. The ideal concentration of NaCl in aqueous solution was determined to be 0.037 M. At low concentrations of NaCl in solution, the adsorption of BPA with a nonplanar and flexible structure greatly increases, and at higher concentrations, it starts to decline. The distribution of the Na⁺ and Cl⁻ ions among the negatively charged graphite platelets may account for this activity, creating a screening effect that facilitates the adsorption of BPA molecules. BPA is less soluble in solution when NaCl is present, and its ability to bind to xGnP is improved. Because Na⁺ and Cl⁻ ions are present, the "butterfly" or lying-down form of BPA may make it easier for more accessible adsorption sites to be occupied. It was shown that the adsorption capacity reduced at concentrations greater than 0.05 M, most likely as a result of competition amongst the species engaged in the process. In this study, equilibrium adsorption was represented by Langmuir, Freundlich, Harkin-Jura, and Temkin isotherms. When the adsorption process approaches equilibrium, the interactions between the adsorbent and the adsorbate are indicated by the adsorption isotherm models. The adsorption of BPA on xGnP most closely resembles the Langmuir isotherm based on a comparison of R² values, indicating a monolayer adsorption system on the surface. The kinetics of the adsorption process were studied using pseudo-first and second order models as well as intraparticle diffusion one. The experimental adsorption capacity, q_e exp (850 mg/g), was in greater agreement with the calculated one based on the pseudo-second order model, according to the results. Due to the large system of graphene, which is a strong electron acceptor, it favours a configuration that allows the interaction with the negatively charged sites of BPA. The physisorption of BPA on graphene is aided by charged controlled interactions in addition to van der Waals interactions; chemisorption is less significant on pure xGnP. The thermodynamic parameters provide

insights as to how the internal energy evolves throughout the adsorption process. A process is exothermic when the change in enthalpy value is negative. The absence of normal free energy denotes a spontaneous process.

Al-Khateeb et al. researched the adsorption and removal characteristics of pharmaceutical pollutants such as aspirin (ASA), acetaminophen (APAP), and caffeine (CAF) onto GNPs from aqueous solutions. The TEM characterization analysis reveals that GNPs have many wrinkles and a transparent, layered structure with a smooth surface. Typically, the specific surface area of the solid adsorbent has a significant impact on the adsorption process. The specific surface area of the GNPs must therefore be determined using nitrogen adsorption/desorption isotherms. The obtained adsorption isotherms were categorized as type IV isotherms. The GNPs' specific surface area was discovered to be 635.2 m²/g. It was studied how the mass of GNPs affected the adsorption patterns of ASA, CAF, and APAP. It found that, when an adsorbent mass of 15.0 mg was used, it was generally observed the percentage of ASA, CAF, and APAP adsorption rose almost linearly with the increase in GNPs mass. This development is mostly attributed to the rise in adsorption surface area brought on by the increased mass of GNPs, which made more active adsorption sites for the molecules ASA, CAF, and APAP molecules available. For the first 10 minutes, the adsorption of these three pharmaceutical pollutants increased over time. At this stage, equilibrium had been reached, with the amounts of ASA and CAF adsorbed being 63.5%, 94.3%, and 87.6%, respectively. The first stage of ASA, CAF, and APAP adsorption took place during the first 10 min of adsorption and was characterized by the high number of active binding sites on the GNPs surface at this time. Adsorption happened fast in this step, which suggests that it was controlled by the process by which the molecules of ASA, CAF, and APAP moved from the bulk phase to the surface of the GNPs. Because there were less active sites available for the ASA, CAF, and APAP molecules on the surface of the GNPs in the second stage, adsorption was probably an attachment-controlled process. It was investigated how pH affected the effectiveness of ASA, CAF, and APAP removal by GNPs. In the case of ASA and CAF,

the pH of the solution did not generally affect the removal of pharmaceutical compounds by GNPs; the percentage of adsorption (70 and 80, respectively) was not considerably affected by changing the pH value. In the case of APAP, raising the pH from 2.0 to 8.0 had no effect on the percentage of adsorption, while raising the pH to 11.0 was linked to a sharp drop in the percentage from 88.7% to 73.8%. The GNPs covered by the negatively charged hydroxide ions and the negatively charged APAP ions, whose pKa value is 9.9, may repel one another due to electrostatic attraction [76].

The electrostatic and hydrophobic interactions between the adsorbate and the solid adsorbent may be influenced by the ionic strength. Therefore, it is essential to research on how ionic strength affects the way that ASA, CAF, and APAP bind to GNPs. Ionic strength has a significant impact on the adsorption of pharmaceutical compounds because it generates a variety of adsorption conditions in which the electrostatic interactions between the pharmaceutical compounds and the surface of the GNPs are either appealing or repellent. An increase in the ionic strength of the solution had no effect on the percentage of ASA adsorption by GNPs. This suggests that the overall adsorption process is not affected by electrostatic contact. Increasing the ionic strength of the solution did, however, significantly increase the percentage of CAF adsorption, which suggests that - stacking between the surface of the GNPs and neutral CAF (pKa = 14.0) has a stronger electrostatic attraction. Pseudo-first-order and pseudo-second-order kinetic models have been proposed in order to understand the mechanisms of adsorption. The pseudo-second-order model was found to have the highest R^2 value for accurately describing the adsorption of ASA, CAF, and APAP by GNPs. The fundamental cause of the adsorption is a contact between the GNPs and the ASA, CAF, and APAP molecules that acts as an electron donor-acceptor. By computing the thermodynamic parameters, the feasibility and spontaneity of the process of ASA, CAF, and APAP adsorption by GNPs were investigated: Changes in enthalpy, entropy, and Gibbs free energy. Enthalpy change values for the adsorption of ASA, CAF, and APAP by GNPs from aqueous solution were negative; 5.42 kJ/mole, 46.6 kJ/mole, and 25.4 kJ/mole,

respectively. The negative numbers demonstrate that ASA, CAF, and APAP are adsorbed by GNPs in an exothermic nature which explains for the decrease in adsorption at higher temperatures. The strength of the enthalpy change points to physical adsorption as compared to chemical adsorption as the likely mechanism for the weak bonding between ASA, CAF, and APAP by GNPs. When ASA, CAF, and APAP were adsorbed onto the surface of the GNPs, the negative values of entropy change, 13.1 J/mole K, 123.0 J/mole K, and 67.3 J/mole K, indicated a decrease in randomness at the GNP/solution interface. The decrease in the degree of freedom of the drug molecules may be the cause of the negative entropy of ASA, CAF, and APAP's adsorption and immobilization on the surface of GNPs. As would be expected from a product-favoured and spontaneous reaction, the free energy change was negative. The adsorption of ASA, CAF, and APAP by GNPs from aqueous solution is represented by the negative values of ΔG° , which are 1.54 kJ/mole, 10.2 kJ/mole, and 5.42 kJ/mole, respectively [76].

Zaka et al. [80] were using a response surface modelling technique to analyse the effect of four distinct parameters on the elimination of levofloxacin (LFX) using GNPs. Extremely acidic and alkaline conditions diminish the effectiveness marginally. It can be noticed that both dosage and time have a positive effect on removal efficiency. If one of the variables is held constant, the trend remains unchanged. This is due to the fact that an increase in dosage will result in a greater number of accessible sites, hence increasing the removal. The change in elimination due to dosage is more important than the change in effect due to time. At any given time, a rise in concentration will result in a decrease in removal efficiency, which could be attributed to active site saturation. Zaka et al. [80] conducted five trials under optimal conditions: contact time = 77 minutes, GNP dosage = 2.1 g/L, pH = 5, and levofloxacin concentration = 10.5 mg/L. These five studies yielded removal efficiencies of 98.29 %, 98.15 %, 98.55 %, 97.97 %, and 98.59 % respectively. To fit the experimental data, three different isotherm models Langmuir, Freundlich, and Temkin were applied. It can be seen that the Langmuir isotherm model, which has an R^2 value of 0.996, best describes

the adsorption of LFX. This shows that the adsorption is monolayer- and homogeneous-based in nature. The experimental model for the removal of LFX using GNPs was fitted using pseudo-first order and pseudo-second order kinetic models. The pseudo-second order model's observed R^2 value of 0.999 was determined to be preferable to the pseudo-first order model's R^2 value of 0.880. Thermodynamic properties including change in Gibbs free energy (ΔG°), change in enthalpy (ΔH°), and change in entropy (ΔS°) were calculated in order to explore the energy changes connected with LFX elimination. It can be shown that the free energy change values vary from -20 to 0 kJ/mol. This leads to the conclusion that LFX is physically adsorbing to GNPs. Additionally, the negative sign shows that the process is spontaneous. Additionally, the rise in Gibbs free energy shows that adsorption is less likely to occur at high temperatures. The process is endothermic, according to the positive sign of enthalpy change (ΔH°). Additionally, the high affinity of the sorbent for the sorbate is linked to the positive value of entropy, which indicates an increase in randomness at the solid/liquid interface [77].

Kerkez-kuyumcu et al. studied the removal of amoxicillin (AA) from aqueous solution using magnetically modified graphene nanoplatelets (M-GNPs). M-GNPs were produced utilizing a selected GNPs by using a co-precipitation technique. The BET specific surface areas of M-GNPs were measured to be 543.2 m²/g. The specific surface area of the GNPs (677.5 m²/g) was significantly higher than that of the M-GNPs, which was decreased upon mixing with the Fe₃O₄ nanoparticles. Up until an adsorbent mass of 5.4 mg was used, the removal % of AA rose almost linearly with increase in M-GNPs mass. According to the study's findings, there was no discernible change in the percentage of amoxicillin removed over the pH range of 3.0 to 5.0, however the percentage clearance decreased when pH rose above 5.0. Amoxicillin is well-known for having three main function groups with different pK_a values: -COOH (pK_{a1} 2.69), -NH₂ (pK_{a2} 7.49), and -OH (pK_{a1} 7.49). (pK_{a3} 9.63). At different pH values, these functional groups ionise to create negatively charged amoxicillin. As the pH of the solution rises, a stronger electrostatic attraction forms between the positively charged surface of the M-GNPs and the negatively

charged amoxicillin. Additionally, competition for the active sites on the surface of the M-GNPs develops as the pH of the solution rises between the negatively charged -OH ions and positively charged amoxicillin ions. A pH of about 5.0 was selected as the ideal value for amoxicillin adsorption onto M-GNPs. Since there are several adsorption circumstances where the electrostatic interactions between the surface of the M-GNPs and the pharmaceutical compounds are either attracting or repulsive, the influence of ionic strength on the adsorption of pharmaceutical compounds was studied. The results show that an increase in KNO₃ concentration from 0.0001 M to 0.001 M did not significantly alter the percentage of adsorption, but an increase to 0.01 M caused a significant decrease in the percentage of adsorption from 68.3% to 33.9%. This happens as a result of the inhibitory effect of a high concentration of K⁺ ions. Last but not least, the ionic strength investigation showed that electrostatic interaction caused by π - π stacking influenced the adsorption behaviour of amoxicillin on M-GNPs solution.

Three different isotherm models—the Langmuir, Freundlich, and Temkin models were used to analyse the adsorption of AA on M-GNPs. The average R^2 values for the Temkin isotherm model and the Langmuir isotherm model were nearly identical ($R^2 > 0.99$). Accordingly, the adsorption mechanism included both monolayer adsorption and electrostatic interaction between the surface and adsorbate through the π - π stacking of electrons, which agreed with the results of the study on ionic strength. The pseudo-second-order model, intraparticle diffusion, and Bangham models were used to analyse the adsorption kinetics. It was determined that the use of M-GNPs for the removal of AA from aqueous solution primarily followed a pseudo-second-order kinetic model, as observed by an excellent correlation coefficient (> 0.99), which confirms that the major cause of AA's adsorption on M-GNPs is to π - π electron donor-acceptor interaction, which is the rate-determining step. In this study, the thermodynamic parameters were analysed; the negative value of ΔG° indicated that the adsorption was spontaneous, the negative value of ΔH° that the process was exothermic, and the negative value of ΔS° that the surface

randomness was decreased as AA molecules adsorb on the adsorbents. Investigations on the recovery and reusability of the adsorbent revealed that it had a great ability to remove AA repeatedly without losing stability [78].

Ion et al. published the first data on phenol removal utilizing exfoliated graphitic nanoplatelets (xGnPs) as a sorbent. They studied the influence of contact time on phenol adsorption. The results demonstrated that phenol adsorption is slow, with the majority of adsorption occurring within the first 10 hours. The equilibrium was reached following 30 hours of adsorption. In addition, the results demonstrated that phenol is better adsorbed on as-grown xGnP than on oxidized xGnP, but equilibrium is reached after the same contact time. Hydrogen bonding is one mechanism for the sorption of phenol and other organic compounds on carbon-based sorbents, but from the data suggest that this process may not be relevant between the phenolic and functional groups on the xGnPs. Possible hydrogen bonding between surface-adsorbed phenol and dissolved phenol may contribute to the increased sorption capacity values found for xGnPs with high surface areas. Moreover, the dissociation of $-OH$ groups on the phenols may hinder the formation of hydrogen bonds between the surface adsorbed on oxidized xGnPs relative to as-grown xGnPs, hence reducing sorption. The π - π electron donor-acceptor interactions have been applied to the adsorption of organic molecules on the graphene surface. As an amphoteric adsorbate, graphene could be extremely polarizable. Hydroxyl is an electron-donating functional group that boosts the π -donating strength of the graphene aromatic ring and the sorption affinity of phenol to the surface of xGnPs. The influence of starting phenol concentration on adsorption efficiency at 400 mg/L xGnP when 72.25 percent phenol removal is accomplished. According to the study, the percentage of phenol adsorption increased as pH rose from 2 to 6 and subsequently reduced as pH approached the phenol pKa. The adsorption of phenol on xGnPs was analysed using Langmuir and Freundlich models. Langmuir sorption isotherm is more applicable to describe phenol adsorption to xGnPs. This is also confirmed by the higher correlation coefficient ($R^2 = 0.985$) in the case of Langmuir model as compared to Freundlich model [74].

Banerjee et al. investigated the potency and effectiveness of graphene oxide nanoplatelets (GONPs) as an adsorbent, as well as its application for the efficient uptake of ibuprofen (IBP) from an aqueous solution. In batch adsorption studies, the various process parameters were investigated in order to determine their effect on the relevant process. Maximum IBP removal (98.17%) was found at an initial IBP concentration of 6 mg/L, adsorbent dosage of 1.00 g/L, solution pH of 6, agitation speed of 180 RPM, and temperature of 308K following 60 minutes of treatment. The adsorbent of GONPs exhibited thin, crinkled, overlapping paper-like structures in intimate association, which represented the distinctive property of single-layer graphene oxide sheets, according to SEM pictures of GONPs. The GONP surface's folded structures gave a larger surface area for more effective adsorption. After being used to adsorb IBP, GONPs' sharp edges notably began to soften. TEM was used to show the surface shape of GONPs before and after IBP adsorption. Images from TEM analysis showed the overlapping GONPs and their stable aqueous phase dispersion, which allows for increased adsorption rates [79].

The adsorption isotherm study was carried out using the Langmuir, Freundlich, Temkin, and Dubinin-Radushkevich isotherm models. $R^2 = 0.994$, the highest correlation coefficient, indicates that the Langmuir model best explains IBP adsorption over GONPs. This indicated the homogeneous nature of the GO and implied that each IBP molecule's binding energy to the surface GO was constant. Thus, it can be inferred that GO molecules did not interact with one another, indicating that IBP molecules formed a monolayer covering on the surface of GO. Intraparticle diffusion, pseudo-first-order, pseudo-second-order, and Elovich models were used to examine the reaction's pathway and any potential rate-limiting phases during the adsorption of IBP by GONPs at various temperatures (293–313 K). The pseudo-second order rate kinetics is thought to best describe IBP adsorption by GONPs based on the highest correlation coefficient values ($R^2 = 0.998$). The Arrhenius equation was used to compute the activation energy (E_a), which was found to be 13.49 kJ/mol. IBP adsorption by GONPs is physisorption in nature because

the E_a value obtained is less than 40 kJ/mol. Furthermore, the endothermic nature of the process was revealed by an increase in the adsorption capacity of GONPs (8.217 - 9.165 mg/g) and a concomitant increase in temperature (293 - 313 K). Adsorption thermodynamics was studied, and the results show that the process reached equilibrium by utilizing energy from the system under consideration. The negative values of ΔG° indicated that the adsorption was spontaneous, while the positive values of ΔH° indicated that the process was endothermic in nature. The increased randomness at the solid/solution interface was assumed to be caused by the translational entropy of the displaced water molecules being higher than that of the released IBP ions, which was supported by the positive value of ΔS° . For the removal and recovery of the IBP compounds for solution, investigation of the GONPs' reusability potential is important. The rate of IBP elimination (%) throughout the course of 10 cycles of adsorption and desorption was practically unchanged for eight cycles and slightly reduced for the final two cycles (97.18 and 95.91%) [79].

Rosli et al. conducted research on the use of GNPs to remove the pharmaceutical pollutants sulfamethoxazole (SMX), an antibiotic, and acetaminophen (ACM), an analgesic, from water. The best adsorbent was chosen from among several different types of GNPs, including C750, C300, M15, and M5, each of which has a different surface area. From this study, it was discovered that C750 (738.44 m²/g) had the maximum surface area, followed by C300 (390.30 m²/g), M15 (61.51 m²/g), and M5 (63.55 m²/g). As mesopores, the pore diameters of C750, C300, M15, and M5 fall within the range of (2–50 nm). A larger zeta potential may indicate better dispersion. Zeta potential measured the electrostatic repulsion between similarly charged particles and thus indicates a degree of dispersion efficiency thus giving information about the tendency of agglomeration. Among the other three GNPs, GNP C300 had the most stable observed zeta potential (50.80 mV). With an absolute value of 20.87 mV, GNP M5 has the lowest tendency to aggregate because it is below the 30 mV threshold. Although C750 has a bigger surface area, the preliminary adsorption investigation of four different types of GNPs indicated that C300 has the maximum

removal effectiveness when compared to other forms of GNPs. Based on zeta potential, C300 has the highest level of stability. Further batch adsorption experiments using C300 were conducted with a number of parameters, including solution pH, GNP concentration, initial SMX concentration, and contact time. The pH of the solution had an impact on GNP C300's capacity to adsorb to both SMX and ACM. The initial pH of the solution rose from 2 to 4, eventually raising the adsorption capacity of SMX onto GNP C300. In contrast, ACM's adsorption capacity and removal efficiency progressively increased from acid to neutral before declining as it increased further. For SMX and ACM, maximum adsorption was found at pH 4 (99.27%) and pH 8 (98.38%), respectively. The removal of SMX molecules was hindered by the rising pH of the solution, which led to a poor adsorption capability at higher pH. Since SMX is a well-known acidic organic chemical with a dissociation constant (pKa) between 1.6 and 5.7, acidic circumstances (pH < pKa) were preferable to basic conditions (pH > pKa) for the removal of the target compound. In other words, they are present in aqueous solution as a protonated form when solution pH is lower than their pKa values. The elimination efficiency rose with the increase in GNP C300 dosage from 5 mg to 60 mg, but the adsorption capacity for both medications decreased. Adsorption sites were fully accessible at low adsorbent dosages, increasing adsorption capacity. In comparison to lower adsorbent dosages, the active sites of the adsorbent that were ready to bind with the medicinal compounds were not fully utilised at larger GNP C300 amounts. Adsorbent may aggregate and there may be a chance for solid particle collisions as GNP C300 levels rise. The initial concentration of SMX and ACM rose in a nearly linear fashion. More adsorbate molecules are accessible for adsorption the higher the starting concentration. Adsorption of SMX and ACM by GNP C300 started out pretty rapidly before slowing down as contact time increased. For the purpose of determining the adsorption equilibrium between the pharmaceuticals and GNP C300, the Langmuir and Freundlich isotherm models were used. The Langmuir isotherm model was shown to have R² values of 0.9952 for SMX and 0.9946 for ACM, indicating a quite better fit and greater suitability for modelling the adsorption of pharmaceuticals onto GNP

C300. This indicated that SMX and ACM adsorption on GNP C300 occurred in a monolayer on a homogeneous surface without contact between the adsorbate. Adsorption kinetics were investigated, and linear regression was used to obtain the kinetic parameters and the correlation coefficient, R^2 . Compared to the pseudo-first-order kinetic models, the pseudo-second-order model fitted the data better. According to the pseudo-second-order model, the correlation coefficients (R^2) for both SMX and ACM were 0.9999, which was higher than the correlation coefficients for the pseudo-first order. Thus, in agreement with chemisorption being the rate-controlling phase, the pseudo-second-order model was better fit for modelling the process of SMX and ACM adsorption on GNP C300. To further describe the diffusion mechanism, the intraparticle diffusion model was used. Data multilinearity suggests that intraparticle diffusion influences the early stages of adsorption but was not the rate-determining step for the entire adsorption process [80].

Badhei et al. worked on adsorption of Metronidazole antibiotic drug (MNAD) onto magnetically modified graphene nanoplatelets (MMGN) from aqueous solution. The MMGNs were prepared by mixing GNPs with freshly prepared magnetite nanoparticles and the new characteristics were further observed during the investigation. The effect of different operational parameters which affect the removal process were explored such as; adsorbent amounts, contact time, initial pH, temperature, and the initial concentration of MNAD. The results showed that the MNAD was removed within 120 min using 9.8 mg adsorbent, at pH 5.0 and 293 K. Adsorption equilibrium data were fitted using both Langmuir and Temkin isotherms, and the Langmuir maximum adsorption capacity was found to be 112.48 mg g⁻¹. Adsorption for MNAD was studied kinetically and thermodynamically, and found to be well fitted by the pseudo second order kinetic model, spontaneous and exothermic in nature. The adsorption behavior of MNAD on MMGN involved π - π stacking and electrostatic interaction, and the rate determining step was the π - π electron donor-acceptor interaction. Recovery, and reusability of the adsorbent was investigated, and the adsorbents showed great ability for the removal of Antibiotic drug for many times without

losing its stability. Generally, MMGN could be considered a potential and promising adsorbent for the removal of organic pollutants from polluted water [1].

de Assis et al. the synthesis of graphene oxide (GO) nanosheets, to be used as adsorbent for the removal of textile dyes from wastewater, was optimized by the modified Hummers method. The GO nanosheets produced were compared with commercial GNPs. The surface area (BET model) for commercial GNPs presented a value of $90.08 \pm 3.01 \text{ m}^2 \text{ g}^{-1}$. No hysteresis was observed, which was expected since the material is nonporous, formed only by nanosheets, often superposed. The surface area of GO synthesized by the modified Hummers method presented a value of $176.00 \pm 2.09 \text{ m}^2 \text{ g}^{-1}$, which indicates that the oxidation of the material is favoring the free surface area. It is estimated that the application of ultrasound techniques can promote exfoliation of the sheets and increase the specific surface area. The results of removal efficiency for the blue dye (SFGL) on the two sorts of adsorbents studied evidenced the anionic behavior of the direct dye, because there was a tendency to the significant increase of the removal efficiency when at pH <4, especially when adsorbed on graphene oxide, reaching efficiency higher than 90% at pH 1.0. This pattern may be due to the functional groups of the dye adsorbed on the surface of the GO which increase its surface complexing ability. Because of the high functionalization of the graphene oxide by hydroxyl (-OH) and carboxylic groups (-COOH), negatively charged in aqueous solution, the presence of available oxygen groups and the arrangement of the active functional groups of the dye species, it is possible to occur stronger chemical bonds, such as hydrogen bonds, between GO and the dyes. The results of the removal efficiency of the dye Red 81 under the two different adsorbents were quite different. When adsorbed on commercial graphene the dye exhibited exceptional high efficiency at low pH, which rapidly decreased at higher pHs. When adsorbed on graphene oxide, the removal efficiency did not reach values higher than 80% for low pH, however for pHs above 7.5 reached efficiency close to 100%. The presence of large amounts of OH- functional groups in the GO may facilitate interaction with the amine -NH functional groups of the dye at higher pHs, resulting in a greater

adsorption at these levels. It suggested that the negatively charged sulfonate groups (SO_3^-) of dye molecule neutralize the electrostatic interaction with oxygen-containing groups on the GO surface, so that of the π - π interactions and the hydrogen bonds with the GO surface can play a dominant role in the adsorption process. Hence, a pH of 3.5 was set to evaluate the influence of the initial dye concentration. Best concentration of 50 ppm for the GO and 100 ppm for the commercial graphene were selected as it resulted in a maximum adsorption capacity [24].

The adsorption isotherm of the dyes Indosol SFGL direct blue and Red 81 on graphene oxide (GO) were studied. Langmuir isotherm fitting best suited both data points, with monolayer maximum sorption capacity (q_m) of 128.58 and 190.53 $\text{mg}\cdot\text{g}^{-1}$ for SFGL and Red 81, respectively, and satisfactory coefficient of determination (R^2) above 0.96. The Freundlich model also showed a satisfactory $R^2 = 0.90$. It were observed that the Red 81 dye is better adsorbed onto GO, when compared to SFGL, showing a higher adsorption capacity for all the concentrations studied. This might be related to strong interactions between the oxygenated function groups of OG and the -NH and -OH groups of the Red 81 dye. The adsorption behavior was best fitted by a pseudo-second order kinetic model. A layer of graphene has a large two-dimensional planar structure; its extended, delocalized π -electron system facilitates interaction with the direct dyes through π - π stacking, low electrostatic interaction, or Van der Waals forces. The simultaneous action of the different adsorption mechanisms present in the interaction between dyes and adsorbents are important for the understanding of the evolution of adsorptive capacity through existing functional groups. The structural properties of GO allow interaction with organic molecules via non-covalent forces such as π - π stacking and hydrogen bonds. The GO surface is negatively charged due to the presence of large numbers of oxygen-containing functional groups, such as epoxy, carboxyl and hydroxyl. With the protonation of the GO surface by acid pH, the number of positively charged sites increases, favoring the adsorption of negatively charged dye ions by attraction forces. Hence, the high removal efficiency at lower pHs for SFGL using this adsorbent. This blue dye has four sulfonic acid

groups ($\text{R-SO}_3\text{Na}$), which, in aqueous medium has the dissociation of sodium ions (Na^+) and sulfonate (R-SO_3^-). However, these sulfonic groups have pK_a less than zero and therefore exhibit negative charges even at lower pHs, which helps in the interaction with the protonated GO surface. This factor also assists in the removal of red dye 81, since it contains two sulfonic acid groups in its structure. Another crucial factor is the presence of carboxyl and hydroxyl groups on the GO surface, which can promote hydrogen bonds with the -OH groups, quite present in the SFGL blue, contributing to a greater adsorption capacity of these dye. Specifically, for the Red 81 dye, the existence of an amine group and a hydroxyl in its structure also allows hydrogen bonds with the -OH and -COOH groups present on the GO surface. At basic pH's the hydroxyl and carboxylic groups of the GO are deprotonated and form their anionic specimens ($-\text{ACOO}^-$ and $-\text{AO}^-$), which are believed to interact via dipole-dipole bonds with the $-\text{RNaO}$ and $-\text{RO}$ groups present in this red dye. This explains the high adsorption of the Red 81 dye onto GO, both in acidic and basic pHs. The Red 81 and SFGL blue dyes have five and seven aromatic rings in one molecule, respectively. Its extended, delocalized π -electron system facilitates interaction with the direct dyes through the π - π stacking interaction. As both dyes exhibit a planar structure, we believe that these π - π stacking are a secondary interaction mechanism between both dyes and GO, and a main interaction mechanism between the dyes and the commercial graphene (as few oxidized functional groups are present). The adsorptive process on the commercial graphene nanosheets surface occurs by low electrostatic interaction or Van der Waals forces. The electrostatic affinity is indicated by the pH through the analysis of the zero-charge point of the adsorbent which consists of the neutral point in the interaction surface. The low adsorptive capacity using commercial graphene as an adsorbent for SFGL can be explained by the absence of functional oxygen groups. It was found that the adsorption mechanism of benzene does not occur through hydrogen bonds, resulting in a lower adsorptive capacity. It is assumed that in acid pH solution, both anionic dyes exhibits repulsion to the liquid medium and consequently a higher affinity to the inert sheets of graphene nanoplatelets, enabling a better fixation of the

dye and consequently higher adsorption capacity [24].

ElHussein et al., studied on removal of carbamazepine (CBZ) from water using UiO-66 and UiO-66/graphene nanoplatelet composite. UiO-66 and graphene nanoplatelet (GNP)/UiO-66 composites were prepared by hydrothermal method. Morphologies of UiO-66 and UiO-66/GNP nanoparticles were investigated by SEM analysis. The images of particles observed to have a shape of crystals are suitable to literature. The crystal shapes are due to ratio of used modulator acid. In this study, particle size distribution of UiO-66 nanoparticles is about 200 nm, UiO-66/GNP nanoparticles is about 700 nm. BET adsorption-desorption isotherms of adsorbents at 77 K were applied, and specific surface area for the UiO-66, and UiO-66/GNP were estimated as 730.6 m²/g, and 910.5 m²/g, respectively. The BJH pore volume of UiO-66 is 0.0462 cm³/g, and pore radius of 1.92 nm. Also, BJH pore volume of UiO-66/GNP is 0.0357 cm³/g, and pore radius of 1.81 nm. UiO-66 and UiO-66/GNP nanoparticles were prepared for CBZ adsorption. Adsorbent dosage is an important adsorption parameter; 1 mg dosage of UiO-66/GNP and 2.5 mg dosage of UiO-66 was selected as optimum dosage adsorbent. 5 mL of adsorbate solution is more appropriate quantity for UiO-66/GNP. CBZ adsorption capacity reaches to 26.46 mg/g if 5 mL of adsorbate solution. 10 mL of solution is better for UiO-66. The pH of CBZ solution was investigated, the results observed that neutral media is better for both of the adsorbents. pKa values of CBZ are 2.3–13.9. Between pH 3 and 10, CBZ protects its neutral form. Acidic and neutral pH values have nearly similar CBZ adsorption capacities on UiO-66. But UiO-66/GNP has very high adsorption capacity at neutral pH value. This result can be connected to GNP surface. Heterogeneity and uncharged surface of GNP is suitable for CBZ adsorption, π - π stacking brings functional addition to GNP. So, UiO-66/GNP nanoparticles is better for CBZ adsorption from water. Non-linear pseudo-first order and pseudo-second order kinetic models were applied. Pseudo-first order R² values of CBZ adsorption on UiO-66/GNP and UiO-66 were 0.92 and 0.97, respectively. R² values of CBZ adsorption on UiO-66/ GNP and UiO-66 for pseudo-second order were 0.96 and 0.98, respectively. Both of the kinetic model can explain kinetic behaviour of the

adsorption systems. The reaction mechanism is directly due to chemical reactions between urea functional group of carbamazepine (C₁₅H₁₆N₂O₃) and adsorbents. Non-linear Langmuir and Freundlich isotherms was applied in this study. According to adjusted R² values, CBZ adsorption on UiO-66 and UiO-66/GNP are compatible with non-linear Langmuir and Freundlich isotherms. Multilayer adsorption occurs between CBZ and adsorbents. And chemical reaction is the main step of adsorption [81].

Luo et al. investigated the efficiency of GNPs as solid-phase extraction (SPE) sorbent for determination of phthalate esters (PAEs) in aqueous solution. To evaluate the enrichment effect of GNPs sorbent, five PAEs including dimethyl phthalate (DMP), diethyl phthalate (DEP), dipropyl phthalate (DPrP), DBP and dicyclohexyl phthalate (DCHP) were selected as model analytes. The operation parameters affecting the extraction efficiency, including eluent solvent and its volume, and the sample volume were optimized. The eluent solvent for SPE operation has important influence on sample recovery. The choice of eluent solvent is mainly based on the chemical property of the target samples and the chromatographic mode used downstream. Since the separation of five PAEs was performed by reverse phase HPLC (RP-HPLC), the eluent solvent should be compatible with common mobile phase used in RP-HPLC, that is, the eluent solvent should be miscible with the mobile phase. It observed that acetonitrile is the most effective eluent for five PAEs, probably resulting from strong interaction between acetonitrile and GNPs due to its property of aprotic solvent. Thus, acetonitrile was selected as eluent in the following studies. In addition, the pH effect on the extraction was also explored and it was found that the pH had no significant influence on the recoveries. To ensure reliable analytical results and high enrichment factor, the maximal sample loading volume of GNPs-based SPE cartridge was explored. It observed that the peak area of each analyte increased with increase of loading sample volume up to 1000 mL, indicating rich adsorbed sites on the surface of GNPs sorbent. 80-101% of recoveries were achieved for the analytes (except DMP) when the sample loading volume was less than 500 mL [82].

Comparison of GNPs sorbent with other commonly used sorbents, including C₁₈ silica, HLB Oasis, Active carbon, and MWCNTs, has been made. To ensure the same level of packing sorbent in the cartridge, different amounts of sorbents were used due to their different densities. C₁₈ silica (100 mg), HLB Oasis (100 mg), Active carbon (50 mg), MWCNTs (50 mg) and GN (30 mg) were packed in 1 mL SPE cartridge. These cartridges were loaded with 200 mL of sample solutions spiked at 100 ng mL⁻¹ five PAEs. To determine the possible breakthrough of sample, the effluent at different stages of loading, washing, and elution was collected and determined by HPLC. Methanol as the eluent solvent was used for C₁₈ silica and HLB Oasis. Active carbon and MWCNTs were eluted by acetonitrile. It highlighted, GNPs sorbent yielded the highest recoveries (85.6-100.9%) among these tested sorbents, although its amount was the smallest (only 30 mg). By comparison, GNPs sorbent observed the best performance in terms of recoveries and adsorption capacity among several sorbents. This is probably due to its unique structure, which results in strong π -stacking interaction with the benzene ring in the molecule of PAEs. In addition, GNPs have some hydrophilic groups such as hydroxyl and carboxyl groups, which can improve the water-wettability of GNPs and enhance the retention of polar compounds. These features make GN an attractive sorbent for PAEs [82].

Al-Khateeb et al. studied on removal of non-steroidal anti-inflammatory drugs (NSAIDs) from water using high surface area graphene nanoplatelets (HSANGs). The NSAIDs drugs; Ketoprofen (KETO), Naproxen (NAP) and Diclofenac sodium salt (DIC), and Ibuprofen (IBU); were used in this study. Adsorption of pharmaceutical pollutants NSAIDs from aqueous solutions by carbon-based adsorbents such as HSANGs might be occurred through the by π - π stacking due to the presence of the π electrons on both of the organic compounds and the HSANGs surface. However, there are many other factors that may affect this type of interaction and consequently affect the removal process. Therefore, the effect of different factors on the interaction between HSANGs and KETO, NAP, DIC, and IBU was explored and studied. The effect of HSANGs mass on the removal of KETO, NAP, DIC, and

IBU was observed. It is found that the increase in the % removal of NSAIDs with the increase of HSANGs mass. 10.0 mg of HSANGs was able to remove most of the NSAIDs compounds. Further increase of HSANGs increased the % removal of NSAIDs using 40.0 mg of the HSANGs. Within 5.0 minutes adsorption of the NSAIDs compounds reached equilibrium. After 5.0 minutes, the removal percentage did not change significantly. It was also observed that the affinity of the NSAIDs compounds towards the HSANGs was different and followed the following order DIC>NAP>KETO>IBU. Also, this observation could be because DIC, NAP, and KETO molecules composed of two benzene rings, whereas IBU composed of one benzene ring, which allowed DIC, NAP, and KETO molecules to interact and adsorbed on the HSANGs through the π - π interaction. Another reason for the affinity of the NSAIDs compounds towards the HSNGs could be due to the molecular weight and consequently the size of the molecule, as the molecular weights of the molecules. The large size of the molecule allowed them to compete effectively for the adsorption on the surface of the HSANGs. The dependence of the removal on the solution pH is a crucial physicochemical factor, which infers the adsorption mechanism at the solid-solution interface. Therefore, the effect of solution pH on the removal of NSAIDs by HSANGs was studied. The results observed the % removal was the highest at pH value of 2.0 NSAIDs and this % removal did not change by raising the solution pH to 4.0 [83].

It is important to study the adsorption process kinetically through the observation of the experimental parameters that may affect the rate of adsorption and, as a result, help attain equilibrium in a fair amount of time in order to comprehend the adsorption and remediation process. The most common and well-known kinetic models, the pseudo-first-order model and the pseudo-second-order model, were used to analyze the adsorption experimental data of KETO, NAP, DIC, and IBU by the HSANGs in order to comprehend the nature of the adsorption process. It observed that, the pseudo-first-order model, was applied to fit the data. However, the adsorption of KETO, NAP, DIC, and IBU by HSANGs was studied using the pseudo-second-order rate equation showed an excellent regression coefficients ($R^2 > 0.99$)

and straight lines were obtained, as well as good fitting to the experimental data. Using two separate models, the liquid film diffusion model and the intra-particle diffusion model, the adsorption rate-controlling mechanism for the adsorption of the KETO, NAP, DIC, and IBU by HSANGs from aqueous solution was studied. Another kinetic model that involves the flow of adsorbate molecules through a liquid film around the solid adsorbent is the liquid film diffusion model. The linear regression coefficients and convergence of the liquid film diffusion model applied to the adsorption data of KETO, NAP, DIC, and IBU by HSANGs were very low. This suggests that the rate-determining stage for the entire adsorption process was not the liquid film diffusion. Only the kinetic data after the first minute of the adsorption were well-converged with respectable linear regression coefficients. The data of KETO, NAP, DIC, and IBU adsorption by HSANGs did not converge, and no straight lines that passed through the origin were found. The intra-particle diffusion is not the rate-determining step, but it is a component of the adsorption mechanism for the adsorption of KETO, NAP, DIC, and IBU by HSANGs, which suggests that the adsorption processes occur in two kinetic steps. NSAIDs under research may have a significant impact on the adsorption process onto HSANGs. Therefore, it is evident that the adsorption processes were regulated by more than one kinetic step, including intra-particle diffusion of the KETO, NAP, DIC, and IBU via HSANGs and liquid film diffusion. The adsorption mechanism is a mixed process because none of the steps is the rate-determining step. Instead, the first linear step within the first minute is the fastest step and is attributed to the diffusion of KETO, NAP, DIC, and IBU molecules to the HSANGs. The second linear portion is a slower process that corresponds to the intra-particle diffusion of the KETO, NAP, DIC, and IBU through the HSANGs. The HSANGs' ability to adsorb the NSAIDs KETO, NAP, DIC, and IBU from an aqueous solution mostly in accordance with the pseudo-second-order kinetic model, as demonstrated by the excellent correlation coefficients (>0.99) and convergence of the experimental data, led to this conclusion. Additionally, the removal process involves several processes, including intra particle diffusion and liquid film diffusion, however none of these steps determine the removal process's rate [83].

The spontaneity of the NSAID adsorption process was studied by thermodynamic analysis. The ΔH° values for the adsorption of KETO, NAP, DIC, and IBU by HSANGs from the aqueous solution were positive; +39.5 kJ/mole, +42.5 kJ/mole, +47.0 kJ/mole, and +27.5 kJ/mole, respectively. The endothermic character of the adsorption of KETO, NAP, DIC, and IBU by HSANGs is confirmed by the positive enthalpy values, which explains why the rate of adsorption increases as the temperature of the solution rises. Additionally, the amount of ΔH° points to a substantial affinity between the physical characteristics of the adsorption and KETO, NAP, DIC, and IBU by HSANGs. During the adsorption and immobilisation of KETO, NAP, DIC, and IBU, the positive values of ΔS° , +144.8 J/mole.K, +159.7 J/mole.K, +184.0 J/mole.K, and +97.1 J/mole.K, revealed a rise in the degree of randomness at the HSANGs/solution interface. According to the negative values of the predicted free energy change, ΔG° , which were, respectively, -3.38 kJ/mole, -4.79 kJ/mole, -7.45 kJ/mole, and -1.23 kJ/mole for the adsorption of KETO, NAP, DIC, and IBU by HSANGs from aqueous solution, the adsorption of KETO, NAP, and DIC. The adsorption of KETO, NAP, DIC, and IBU by HSANG's process is proposed to be an entropy-driven process by the negative values of ΔG° and the positive values of ΔH° and ΔS° . To determine whether the suggested solid adsorbent is practical, the removal of by HSANGs from actual environmental water samples was examined. For this study, two actual samples were chosen: KETO, NAP, DIC, and IBU tap water (TW), as well as wastewater from King Abdulaziz University Wastewater (WW). The initial KETO, NAP, DIC, and IBU concentrations were tested and were below the HPLC's detection limit, showing that these pollutants were not present in the chosen real water samples. It demonstrates that the majority of NSAIDs such KETO, NAP, DIC, and IBU were eliminated from the WW, and TW spiking samples support the usefulness of HSANGs for environmental remediation, particularly in the case of NSAID pollution. Using actual water samples containing KETO, NAP, DIC, and IBU, the applicability of the HSANGs for the removal of NSAIDs was tested, and the findings demonstrated the high removal effectiveness [83].

Bhattacharya et al. investigates the potential of graphene oxide nanoplatelets (GONPs) for removal of a common and extensively used drug, Carbamazepine (CBZ) from aqueous solutions. The surface morphology of GONP as recorded using SEM observed that the SEM images of GONP composed of thin, closely associated and highly overlapping platelet-like carbon sheets. The rough surfaces of these crumpled GONPs reportedly facilitate efficient adsorption. These wrinkled and layered structures of GO are reportedly formed as a result of interactions between oxygen containing functional groups. Batch studies were performed to assess the potential of graphene oxide for adsorption of CBZ under different. A maximum adsorbate removal of 99% was recorded from a solution containing 5 ppm of CBZ under optimized conditions of solution pH (2), adsorbent dosage (1gL^{-1}), temperature (35°C) and contact time (120 min). Different isotherms models such the Langmuir, Freundlich, Temkin, and Dubinin-Radushkevich were fitted to the percentage CBZ removal. The values of $R^2 = 0.815$ suggested that the results from batch experiments were the most closely related to the Temkin isotherm. Therefore, it may be assumed that CBZ was uniformly adsorbable by GONP. Additionally, this implied that the adsorbent moieties' heat of adsorption reduced linearly as the process advanced. For the examination of process kinetics, CBZ removals were fitted to various models. The pseudo-second order kinetic model best fit the results from batch investigations. The Arrhenius equation was used to compute the activation energy (E_a), which was discovered to be 78 kJ/mol for the adsorption of CBZ by GONPS. The CBZ adsorption by GONP was likely chemisorption in nature if the E_a value was greater than 40 kJ/mol . According to the findings of the study on process thermodynamics, negative values observed for ΔG° suggested the process in question was spontaneous. Additionally, the process' endothermic character was confirmed by the positive figure for enthalpy. Additionally, the positive value for entropy indicated that the translational entropy of the released CBZ ions was lower than that of the water molecules that were displaced, leading to a higher level of unpredictability at the interface between the adsorbent and adsorbate. The CBZ adsorption efficiency of GONP was observed to maintain the same for eight consecutive cycles and fall

in the last two cycles (95 and 90% removal efficiency, respectively), according to the study's findings on reusability. This had happened because of handling-related bulk loss or repeated regeneration-related adsorbent surface degradation [84].

Khalil et al., studied on nanostructured porous graphene (PG) for efficient removal of emerging contaminants (ECs) pharmaceutical; atenolol (ATL), carbamazepine (CBZ), ciprofloxacin (CIP), diclofenac (DCF), gemfibrozil (GEM) and ibuprofen (IBP) from water. Detailed batch tests were conducted to investigate the effects of adsorption time, initial EC concentration, PG dosage, solution pH, and temperature. A maximum adsorbate removal of ECs $>99.9\%$ was recorded from a solution containing 250 ppm of ECs under optimized conditions of solution pH (2), adsorbent dosage (5 mg), and contact time (60 min). To illustrate the sorption mechanism and the role of surface area and active sites, four kinetic models including pseudo-first order, pseudo-second order, Elovich and intraparticle diffusion reaction models were applied to evaluate the rate of adsorption reaction and its rate controlling step. Of the four suggested models, the pseudo-second order rate model best described the kinetics of ECs adsorption onto graphene oxide (GO) and PG with an excellent fit as indicated by the highest correlation coefficient values ($R^2 = 0.99$ for most ECs). The results indicated further affinity of ECs of hydrophilic nature, such as ATL and CIP towards GO, while the other ECs were more attracted to PG. In general, although the adsorption performance of GO was higher for ATL and CIP removal, but, in terms of super hydrophobicity, ease of separation from water, recyclability and chemical stability, PG is a more attractive candidate for ECs removal in water treatment applications [85].

Seven adsorption isotherm models were compared for their potential to best fit the experimental data in order to better clarify. The Freundlich model might be used to represent the adsorption findings of GO for ATL and CBZ in terms of the best match criterion (R^2). The Freundlich isotherm models plausible for explaining heterogeneous multilayer adsorption. The Langmuir isotherm is used to illustrate the IBP adsorption data for GO and PG. This implied that a monolayer coverage

formed in the event of IBP adsorption onto a graphene-based material (GBM) surface, suggesting that the binding energies of each IBP molecule on the surface GO were uniform. Therefore, it can be said that no interactions between GO molecules occurred during the IBP adsorption. Finally, it was discovered that the Langmuir models fairly produced a better fitting than the other models in the instance of DCF adsorbed by GO and PG. The pseudo-second order model was applied as best to described the kinetics of ECs adsorption onto GO and PG with an excellent fit ($R^2 = 0.99$ for most ECs). In every situation, the type of adsorption may be predicted based on the principal adsorption energy E (kJ/mol), which is connected to the D-R model. The ECs' adsorption process on GO and PG showed physical properties, as evidenced by the low values of the E

parameter that were observed. The exothermic character of the adsorption is confirmed by the negative values of ΔH , which explains why adsorption decreases at increasing temperatures. In contrast to chemical adsorption, which has a range of -400 to -80 kJ/mol, the magnitude of ΔH points to a weak type of bonding between ECs by PG, such as physical adsorption (ΔH range between -20 and -40 kJ/mol). The decrease in degree of freedom of pharmaceutical molecules, as indicated by the negative values of ΔS , is thought to be the cause of the decrease in randomness. The free energy change, ΔG , is negative, indicating an enthalpy-driven process and a product-favorable spontaneous reaction. Finally, after being regenerated and used four times to cure pharmaceutically contaminated solutions, PG showed good promise for recycling[85].

Table 1. Summarize of adsorption of EDCs onto graphene nanoplatelets

Adsorbent	Pollutant	Adsorption Isotherm Model	Adsorption Kinetics Model	Adsorption Thermodynamic	Remarks	Ref.
Graphene Nanoplatelets	DCS	Langmuir	Pseudo-second-order	Exothermic and spontaneous process	At pH conditions greater than 4.2, diclofenac sodium ionizes given a negatively charged ion that is electrostatically repelled by GNP surface causes a decrease in the removal efficiency.	[75]
Exfoliated Graphene Nanoplatelets	BPA	Langmuir Freundlich	Pseudo-second-order	Exothermic and spontaneous process	At pH from 3 to 7, the adsorption of BPA slightly increased, than it begins to decrease between 7 and 9.	[29]
Graphene nanoplatelets	ASA, APAP, CAF	BET	Pseudo-second-order	Exothermic spontaneous process and increase in randomness	The percentage of adsorption of CAF was slightly enhanced by increasing the ionic strength of the solution	[76]
Graphene Nanoplatelets	LFX	Langmuir	Pseudo-second-order	Endothermic, spontaneous process and	The dosage and time have a positive effect on removal efficiency.	[77]

				increase in randomness	If one of the variables is held constant, the trend remains unchanged.	
Magnetically modified graphene nanoplatelets	AA	Langmuir Temkin	Pseudo-second-order	Exothermic and spontaneous process and decrease in randomness	These functional groups in AA ionize at various pH levels to produce negatively charged AA; the electrostatic repulsion increases between amoxicillin and M-GNPs surface as the solution pH rises. The hydrogen bonding between surface-adsorbed phenol and dissolved phenol may contribute to the increased sorption capacity values for xGnPs.	[78]
Exfoliated Graphene Nanoplatelets	Phenol	Langmuir				[74]
Graphene Oxide Nanoplatelets	IBP	Langmuir	Pseudo-second-order	Endothermic, spontaneous process and increase in randomness	Maximum IBP removal was found at an initial IBP concentration of 6 mg/L, adsorbent dosage of 1.00 g/L, solution pH of 6, agitation speed of 180 RPM, and temperature of 308K following 60 minutes of treatment.	[79]
Graphene Nanoplatelets	ACM, SMX	Langmuir	Pseudo-second-order		Maximum adsorption was observed at pH 4 (99.27%) for SMX and ACM at pH 8 (98.38%).	[80]
Magnetically Modified Graphene Nanoplatelets	MNAD	Langmuir Temkin	Pseudo-second-order	Exothermic and spontaneous process	MNAD was removed within 120 min using 9.8 mg adsorbent, at pH 5.0 and 293 K.	[1]
Graphene Oxide (GO) Nanosheets, Commercial	Dyes	Langmuir Freundlich	Pseudo-second-order		Dye adsorbed on commercial graphene shows high efficiency at low pH, which	[24]

Graphene					rapidly decreased at higher pH.	
UiO-66, UiO-66/graphene nanoplatelet composite	CBZ	Langmuir Freundlich	Pseudo-first-order Pseudo-second-order		Neutral pH of CBZ solution is better for both of the adsorbents.	[81]
Graphene Nanoplatelets	PAEs				GNPs sorbent yielded the highest recoveries (85.6–100.9%), although its amount was the smallest (only 30 mg).	[82]
High Surface Area Graphene Nanoplatelets	NSAIDs		Pseudo-first-order	Endothermic, spontaneous process and increase at randomness	Percentage removal was the highest at pH value of 2.0 NSAIDs and this % removal did not change by raising the solution pH to 4.0.	[83]
Graphene Oxide Nanoplatelets	CBZ	Temkin	Pseudo-second-order	Endothermic, spontaneous process and increase at randomness	A maximum adsorbate removal of 99% was recorded from a solution containing 5 ppm of CBZ under optimized conditions of solution pH (2), adsorbent dosage (1 gL^{-1}), temperature (35°C) and contact time (120min).	[84]
Nanostructured Porous Graphene	ATL, CBZ, CIP, DCF, GEM, IBP	Freundlich (ATL, CBZ) Langmuir (IBP, DCF) Toth (CIP, GEM, DCF)	Pseudo-second-order	Exothermic, spontaneous process and decrease at randomness	A maximum adsorbate removal of these pharmaceuticals > 99.9% was recorded from a solution containing 250 ppm of ECs under optimized conditions of solution pH (2), adsorbent dosage (5 mg), and contact time (60min).	[85]

Abbreviations: DCS: diclofenac sodium; BPA: bisphenol A; ASA: aspirin; APAP: acetaminophen; CAF: caffeine; LFX: levofloxacin; AA: amoxicillin; SMX: sulfamethoxazole; ACM: acetaminophen; MNAD: metronidazole antibiotic drug; PAEs: phthalate esters; NSAIDs: non-steroidal anti-inflammatory drugs; ATL: atenolol; CBZ: carbamazepine; CIP: ciprofloxacin; DCF: diclofenac; GEM: gemfibrozil; IBP: ibuprofen

Over the decades, the research involving the usage of GNPs have progressed in a multitude of directions. The literatures published in area of nanomaterials governing graphene-based materials especially GNPs indicate the intensity of research activities being carried with this material. The properties of GNPs have caused the wide range of application such as sorbent material for wastewater treatment. However, more research is needed to improve the capability of GNPs to adsorb adsorbates at even lower concentrations. It can be done by further fabricating the GNPs with other materials.

Conclusion

The effective use of graphene nanoplatelets as an adsorbent material for the removal of heavy metals and endocrine disruptors in wastewaters is summarized in this review paper. Pollutants become harmful when exposed for a long period of time, endangering not just humans and the environment but also aquatic life. The conventional treatment techniques might not be sufficient to completely remove these pollutants. Adsorption using graphene materials can be thought of as a simple and low-cost technique, especially for treating distinctive wastes like heavy metals and EDCs, which may only be present in very low concentrations and are harmful if not completely removed. The use of graphene nanoplatelets and its modifications for the removal of heavy metal pollutants and EDCs have made recent progress, as shown in this review. It is evident that graphene nanoplatelets offer a promising alternative to other commonly used adsorbent materials. It has been demonstrated that graphene nanoplatelets have the potential to be one of the most reliable and versatile materials for wastewater treatment in the future. It is important to understand that the adsorptive capacity of graphene nanoplatelets depends on the conditions of the experiment. The results of the batch experiments indicated that the adsorption process was affected by adsorbent dose, contact time, initial phosphate concentration, and temperature. The kinetic study indicated adsorption was governed by several mechanisms with various processes dominating different stages of adsorption. Isotherm studies showed the adsorption could be described by Langmuir, Freundlich, Temkin, and Dubinin-Radushkevich

isotherms. Based on a comparison of the R^2 values, the adsorption onto GNPs adsorbent mostly closely fit Langmuir isotherm, suggesting a monolayer adsorption system on the surface. The kinetic studies included a pseudo-first order kinetic model of a Lagergren curve, a pseudo-second order model and an intra-particle diffusion model to elucidate the adsorption mechanisms and the adsorption control rates was studied. Besides that, the mechanisms of adsorption include chemical and physical interactions was investigated in this review. The present review investigates the significance of thermodynamic parameters, standard free energy change (ΔG°), standard enthalpy change (ΔH°) and standard entropy change (ΔS°) to predict the spontaneity of adsorption of metals and EDCs onto the surface of adsorbents. On the basis of its chemical and structural stability, the GNPs could become a very good adsorbent with applications for water remediation. More studies should be carried out for low-cost adsorption process to promote large scale use of non-conventional adsorbents. Low-cost adsorbents should be used to minimize cost and maximize heavy metal removal efficiency.

References

1. Badhei, S., & Mitra, J. C. Efficient use of graphene nano platelets for removal of antibiotic drug from aqueous solution.
2. Sarmah, A. K., Northcott, G. L., Leusch, F. D. L. and Tremblay, L. A. (2006). A survey of endocrine disrupting chemicals (EDCs) in municipal sewage and animal waste effluents in the Waikato region of New Zealand. *Science of the Total Environment*, 355(1-3): 135-144.
3. Lyssimachou, A., Bachmann, J. and Porte, C. (2008). Short-term exposure to the organotin compound triphenyltin modulates esterified steroid levels in females of *Marisa cornuarietis*. *Aquatic Toxicology*, 89(2): 129-135.
4. Kavlock, R. J. (1999). Overview of endocrine disruptor research activity in the United States. *Chemosphere*, 39(8): 1227-1236.
5. Rusu, C., Preda, C., Sireteanu, A. and Vulpoi, C. (2015). Risk factors in autism spectrum disorders: the role of genetic, epigenetic, immune and environmental interactions. *Environmental*

- Engineering & Management Journal*, 14(4): 901-907.
6. Apul, O. G., Wang, Q., Zhou, Y. and Karanfil, T. (2013). Adsorption of aromatic organic contaminants by graphene nanosheets: Comparison with carbon nanotubes and activated carbon. *Water Research*, 47(4): 1648-1654.
7. Ji, L., Chen, W., Duan, L. and Zhu, D. (2009). Mechanisms for strong adsorption of tetracycline to carbon nanotubes: a comparative study using activated carbon and graphite as adsorbents. *Environmental Science & Technology*, 43(7): 2322-2327.
8. Maliyekkal, S. M., Sreeprasad, T. S., Krishnan, D., Kouser, S., Mishra, A. K., Waghmare, U. V. and Pradeep, T. (2013). Graphene: a reusable substrate for unprecedented adsorption of pesticides. *Small*, 9(2): 273-283.
9. Pavagadhi, S., Tang, A. L. L., Sathishkumar, M., Loh, K. P. and Balasubramanian, R. (2013). Removal of microcystin-LR and microcystin-RR by graphene oxide: adsorption and kinetic experiments. *Water Research*, 47(13): 4621-4629.
10. Geim, A. K. and Novoselov, K. S. (2007). The rise of graphene. *Nature Materials*, 6(3): 183-191.
11. Stoller, M. D., Park, S., Zhu, Y., An, J. and Ruoff, R. S. (2008). Graphene-based ultracapacitors. *Nano Letters*, 8(10): 3498-3502.
12. Afsahi, S., Lerner, M. B., Goldstein, J. M., Lee, J., Tang, X., Bagarozzi Jr, D. A., ... and Goldsmith, B. R. (2018). Novel graphene-based biosensor for early detection of Zika virus infection. *Biosensors and Bioelectronics*, 100: 85-88.
13. Nayak, G. S., Zybala, R., Kozinski, R., Woluntarski, M., Telle, R. and Schickle, K. (2018). Immobilization of reduced graphene oxide nanoflakes on inert ceramic surfaces using self-assembled monolayer technique. *Materials Letters*, 225: 109-112.
14. Bai, R. G., Ninan, N., Muthoosamy, K. and Manickam, S. (2018). Graphene: A versatile platform for nanotheranostics and tissue engineering. *Progress in Materials Science*, 91: 24-69.
15. Chan, K. K., Yap, S. H. K. and Yong, K. T. (2018). Biogreen synthesis of carbon dots for biotechnology and nanomedicine applications. *Nano-Micro Letters*, 10: 1-46.
16. Partoens, B. and Peeters, F. M. (2006). From graphene to graphite: Electronic structure around the K point. *Physical Review B*, 74(7): 075404.
17. Wan, Q., Cai, H., Liu, Y., Song, H., Liao, H., Liu, S. and Yang, N. (2013). Graphene nanoplatelets: Electrochemical properties and applications for oxidation of endocrine - disrupting chemicals. *Chemistry - A European Journal*, 19(10): 3483-3489.
18. Choi, W., Lahiri, I., Seelaboyina, R. and Kang, Y. S. (2010). Synthesis of graphene and its applications: a review. *Critical Reviews in Solid State and Materials Sciences*, 35(1): 52-71.
19. Pumera, M. (2009). Electrochemistry of graphene: New horizons for sensing and energy storage. *The Chemical Record*, 9(4): 211-223.
20. Sadanala, K. C. and Chung, B. C. (2013). Graphene nanoplatelets as a solid phase extraction sorbent for analysis of chlorophenols in water. *Journal of the Korean Society for Applied Biological Chemistry*, 56: 673-678.
21. Geng, Y., Wang, S. J. and Kim, J. K. (2009). Preparation of graphite nanoplatelets and graphene sheets. *Journal of Colloid and Interface Science*, 336(2): 592-598.
22. Kumar, R., Pandey, K. K., Islam, A. and Keshri, A. K. (2019). Graphene nanoplatelets: A promising corrosion inhibitor and toughening inclusion in plasma sprayed cerium oxide coating. *Journal of Alloys and Compounds*, 809: 151819.
23. Liu, J., Dong, J., Zhang, T. and Peng, Q. (2018). Graphene-based nanomaterials and their potentials in advanced drug delivery and cancer therapy. *Journal of Controlled Release*, 286: 64-73.
24. de Assis, L. K., Damasceno, B. S., Carvalho, M. N., Oliveira, E. H. and Ghislandi, M. G. (2019). Adsorption capacity comparison between graphene oxide and graphene nanoplatelets for the removal of coloured textile dyes from wastewater. *Environmental Technology*, 41: 2360-2371.
25. Cataldi, P., Athanassiou, A. and Bayer, I. S. (2018). Graphene nanoplatelets-based advanced materials and recent progress in sustainable applications. *Applied Sciences*, 8(9): 1438.

26. An, J. C., Lee, E. J., Yoon, S. Y., Lee, S. Y. and Kim, Y. J. (2018). Comparative study on the morphological properties of graphene nanoplatelets prepared by an oxidative and non-oxidative route. *Carbon Letters*, 26: 81-87.
27. Huang, Z. H., Zheng, X., Lv, W., Wang, M., Yang, Q. H. and Kang, F. (2011). Adsorption of lead (II) ions from aqueous solution on low-temperature exfoliated graphene nanosheets. *Langmuir*, 27(12): 7558-7562.
28. Ion, A. C., Ion, I. and Culetu, A. (2011). Lead adsorption onto exfoliated graphitic nanoplatelets in aqueous solutions. *Materials Science and Engineering: B*, 176(6): 504-509.
29. Radu, E., Catrinel Ion, A., Sirbu, F. and Ion, I. (2015). Adsorption of endocrine disruptors on exfoliated graphene nanoplatelets. *Environmental Engineering & Management Journal*, 14(3): 551-558.
30. Ahmad, H., Laini, V. V., Qian, T. Z., Jelani, R. M., Rosli, F. A. and Kamaruzaman, S. (2020). Efficient removal of lead from aqueous using hybrid graphite nanoflakes/mesoporous silica nanoparticles, amine functionalized mesoporous silica and graphite nanoflakes as adsorbents. *Malaysian Journal Analytical Sciences*, 24: 236-246.
31. Briffa, J., Sinagra, E. and Blundell, R. (2020). Heavy metal pollution in the environment and their toxicological effects on humans. *Heliyon*, 6(9): 04691.
32. Ali, H., Khan, E. and Ilahi, I. (2019). Environmental chemistry and ecotoxicology of hazardous heavy metals: environmental persistence, toxicity, and bioaccumulation. *Journal of Chemistry*, 2019: 6730305.
33. Sall, M. L., Diaw, A. K. D., Gningue-Sall, D., Efremova Aaron, S. and Aaron, J. J. (2020). Toxic heavy metals: Impact on the environment and human health, and treatment with conducting organic polymers, a review. *Environmental Science and Pollution Research*, 27: 29927-29942.
34. Nguyen, P. Y., Silva, A. F., Reis, A. C., Nunes, O. C., Rodrigues, A. M., Rodrigues, J. E., ... and Carvalho, G. (2019). Bioaugmentation of membrane bioreactor with *Achromobacter denitrificans* strain PR1 for enhanced sulfamethoxazole removal in wastewater. *Science of the Total Environment*, 648: 44-55.
35. Sharma, G., Gupta, V. K., Agarwal, S., Bhogal, S., Naushad, M., Kumar, A. and Stadler, F. J. (2018). Fabrication and characterization of trimetallic nano-photocatalyst for remediation of ampicillin antibiotic. *Journal of Molecular Liquids*, 260: 342-350.
36. Kumar, A., Kumar, A., Sharma, G., Ala'a, H., Naushad, M., Ghfar, A. A. and Stadler, F. J. (2018). Quaternary magnetic BiOCl/g-C₃N₄/Cu₂O/Fe₃O₄ nano-junction for visible light and solar powered degradation of sulfamethoxazole from aqueous environment. *Chemical Engineering Journal*, 334: 462-478.
37. Thakur, A., Kumar, P., Kaur, D., Devunuri, N., Sinha, R. K. and Devi, P. (2020). TiO₂ nanofibres decorated with green-synthesized P Au/Ag@CQDs for the efficient photocatalytic degradation of organic dyes and pharmaceutical drugs. *RSC Advances*, 10(15): 8941-8948.
38. Hemmat, K., Khodabakhshi, M. R. and Zeraatkar Moghaddam, A. (2021). Synthesis of nanoscale zerovalent iron modified graphene oxide nanosheets and its application for removing tetracycline antibiotic: Response surface methodology. *Applied Organometallic Chemistry*, 35(1): e6059.
39. Liu, Q., Li, L., Jin, X., Wang, C. and Wang, T. (2018). Influence of graphene oxide sheets on the pore structure and filtration performance of a novel graphene oxide/silica/polyacrylonitrile mixed matrix membrane. *Journal of Materials Science*, 53(9): 6505-6518.
40. de Matos Rodrigues, M. H., de Sousa, P. A. R., Borges, K. C. M., de Melo Coelho, L., de Fátima Gonçalves, R., Teodoro, M. D., ... and Júnior, M. G. (2019). Enhanced degradation of the antibiotic sulfamethoxazole by heterogeneous photocatalysis using CeO₂, 8GdO₃, 2O₂-δ/TiO₂ particles. *Journal of Alloys and Compounds*, 808: 151711.
41. Hu, L., Zhang, Y., Lu, W., Lu, Y. and Hu, H. (2019). Easily recyclable photocatalyst Bi₂WO₆/MOF/PVDF composite film for efficient degradation of aqueous refractory organic pollutants under visible-light irradiation. *Journal of*

- Materials Science*, 54: 6238-6257.
42. Tang, J. and Wang, J. (2020). Iron-copper bimetallic metal-organic frameworks for efficient Fenton-like degradation of sulfamethoxazole under mild conditions. *Chemosphere*, 241: 125002.
 43. Zhuan, R. and Wang, J. (2020). Enhanced degradation and mineralization of sulfamethoxazole by integrating gamma radiation with Fenton-like processes. *Radiation Physics and Chemistry*, 166: 108457.
 44. Xu, J., Xu, W., Wang, D., Sang, G. and Yang, X. (2016). Evaluation of enhanced coagulation coupled with magnetic ion exchange (MIEX) in natural organic matter and sulfamethoxazole removals: the role of Al-based coagulant characteristic. *Separation and Purification Technology*, 167: 70-78.
 45. Delgado, N., Capparelli, A., Navarro, A. and Marino, D. (2019). Pharmaceutical emerging pollutants removal from water using powdered activated carbon: study of kinetics and adsorption equilibrium. *Journal of Environmental Management*, 236: 301-308.
 46. Xiao, F. Z., Wang, C., Yu, L. M., Pu, Y. Q., Xu, Y. L., Zhang, K., ... and He, S. Y. (2019). Fabrication of magnetic functionalised calix [4] arene composite for highly efficient and selective adsorption towards uranium (VI). *Environmental Chemistry*, 16(8): 577-586.
 47. Moghaddam, A. Z., Esmaeilkhani, E. and Shakourian-Fard, M. (2019). Immobilizing magnetic glutaraldehyde cross-linked chitosan on graphene oxide and nitrogen-doped graphene oxide as well-dispersible adsorbents for chromate removal from aqueous solutions. *International Journal of Biological Macromolecules*, 128: 61-73.
 48. Patel, M., Kumar, R., Kishor, K., Mlsna, T., Pittman Jr, C. U. and Mohan, D. (2019). Pharmaceuticals of emerging concern in aquatic systems: chemistry, occurrence, effects, and removal methods. *Chemical Reviews*, 119(6): 3510-3673.
 49. Carmalin Sophia, A., Lima, E. C., Allaudeen, N. and Rajan, S. (2016). Application of graphene based materials for adsorption of pharmaceutical traces from water and wastewater-a review. *Desalination and Water Treatment*, 57(57): 27573-27586.
 50. Kucherovala, A., Burakova, I. and Burakov, A. (2017). Graphene materials for lead(II) extraction: an equilibrium study. In *MATEC Web of Conferences*. EDP Sciences, 129: 06022.
 51. Mishra, A. K. and Ramaprabhu, S. (2011). Removal of metals from aqueous solution and sea water by functionalized graphite nanoplatelets based electrodes. *Journal of Hazardous Materials*, 185(1): 322-328.
 52. Sheng, Z., Cao, M., Hong, Y., Wang, S., Fan, Z., Xiong, J., ... and Deng, C. (2018). Preparation of functionalized graphene nano-platelets and use for adsorption of Pb²⁺ from solution. *Journal of Wuhan University of Technology-Materials Science Edition*, 33(6): 1395-1401.
 53. Nandi, D., Ghosh, S. K., Ghosh, A., Siengchin, S., Roy, A., Gupta, K., ... and Ghosh, U. C. (2021). Arsenic removal from water by graphene nanoplatelets prepared from nail waste: A physicochemical study of adsorption based on process optimization, kinetics, isotherm and thermodynamics. *Environmental Nanotechnology, Monitoring & Management*, 16: 100564.
 54. Zhu, J., Sadu, R., Wei, S., Chen, D. H., Haldolaarachchige, N., Luo, Z., ... and Guo, Z. (2012). Magnetic graphene nanoplatelet composites toward arsenic removal. *ECS Journal of Solid State Science and Technology*, 1(1): M1.
 55. Samaraweera, H., Pittman Jr, C. U., Thirumalai, R. V. K., Perez, F. and Misna, T. (2021). Characterization of graphene/pine wood biochar hybrids: Potential to remove aqueous Cu²⁺. *Environmental Research*, 192: 110283.
 56. Rosenzweig, S., Sorial, G. A., Sahle-Demessie, E. and McAvoy, D. C. (2014). Optimizing the physical-chemical properties of carbon nanotubes (CNT) and graphene nanoplatelets (GNP) on Cu(II) adsorption. *Journal of Hazardous Materials*, 279: 410-417.
 57. Capra, L., Manolache, M., Ion, I., Stoica, R., Stinga, G., Doncea, S. M., ... and Ion, A. C. (2018). Adsorption of Sb(III) on oxidized exfoliated graphite nanoplatelets. *Nanomaterials*, 8(12): 992.
 58. Smith, D. M., Hamwi, B. and Rogers, R. E. (2022). Carbon nanomaterial-based aerogels for improved removal of copper(II), zinc(II), and lead(II) ions

- from water. *Environmental Science: Advances*, 1(2): 208-215.
59. Bogdan, D., Rizea, G. A., Ion, I. and Ion, A. C. (2016). Ammonium adsorption on exfoliated graphite nanoplatelets. *Revista de Chimie*, 67: 2231-2236.
60. Yin, Q., Zhu, Y., Ju, S., Liao, W. and Yang, Y. (2016). Rapid determination of copper and lead in *Panax notoginseng* by magnetic solid-phase extraction and flame atomic absorption spectrometry. *Research on Chemical Intermediates*, 42: 4985-4998.
61. La, D. D., Patwari, J. M., Jones, L. A., Antolasic, F. and Bhosale, S. V. (2017). Fabrication of a GNP/Fe-Mg binary oxide composite for effective removal of arsenic from aqueous solution. *ACS Omega*, 2(1): 218-226.
62. Li, B.-Q., Yuan, W., and Li, L. (2016). Adsorption of Pb^{2+} and Cd^{2+} on graphene nanosheets prepared using thermal exfoliation. *Acta Physico-Chimica Sinica*, 32: 997-1004.
63. Kucherovala, A. E., Romantsova, I. V., Burakov, A. E., Memetov, N. R. and Krasnyansky, M. N. (2017). Graphene-based nanocomposites for enhanced Pb^{2+} adsorption. *Nano Hybrids and Composites*, 13: 323-329.
64. Kumar, A. K., Sarma, P. N. and Mohan, S. V. (2016). Incidence of selected endocrine disrupting estrogens in water bodies of Hyderabad and its relation to water quality parameters. *Environmental Engineering Management Journal*, 15: 315-325.
65. Ternes, T. A., Stumpf, M., Mueller, J., Haberer, K., Wilken, R. D. and Servos, M. (1999). Behavior and occurrence of estrogens in municipal sewage treatment plants—I. Investigations in Germany, Canada and Brazil. *Science of The Total Environment*, 225(1-2): 81-90.
66. Shi, J., Fujisawa, S., Nakai, S. and Hosomi, M. (2004). Biodegradation of natural and synthetic estrogens by nitrifying activated sludge and ammonia-oxidizing bacterium *Nitrosomonas europaea*. *Water Research*, 38(9): 2323-2330.
67. Auriol, M., Filali-Meknassi, Y., Adams, C. D. and Tyagi, R. D. (2006). Natural and synthetic hormone removal using the horseradish peroxidase enzyme: temperature and pH effects. *Water research*, 40(15), 2847-2856.
68. Filali-Meknassi, Y., Tyagi, R. D., Surampalli, R. Y., Barata, C. and Riva, M. C. (2004). Endocrine-disrupting compounds in wastewater, sludge-treatment processes, and receiving waters: Overview. *Practice Periodical of Hazardous, Toxic, and Radioactive Waste Management*, 8(1): 39-56.
69. Jobling, S., Nolan, M., Tyler, C. R., Brighty, G. and Sumpter, J. P. (1998). Widespread sexual disruption in wild fish. *Environmental Science & Technology*, 32(17): 2498-2506.
70. Kumar, A. K. and Mohan, S. V. (2012). Removal of natural and synthetic endocrine disrupting estrogens by multi-walled carbon nanotubes (MWCNT) as adsorbent: kinetic and mechanistic evaluation. *Separation and Purification Technology*, 87: 22-30.
71. Pojana, G., Gomiero, A., Jonkers, N. and Marcomini, A. (2007). Natural and synthetic endocrine disrupting compounds (EDCs) in water, sediment and biota of a coastal lagoon. *Environment International*, 33(7): 929-936.
72. Routledge, E. J. and Sumpter, J. P. (1996). Estrogenic activity of surfactants and some of their degradation products assessed using a recombinant yeast screen. *Environmental Toxicology and Chemistry: An International Journal*, 15(3): 241-248.
73. Snyder, S. A., Villeneuve, D. L., Snyder, E. M. and Giesy, J. P. (2001). Identification and quantification of estrogen receptor agonists in wastewater effluents. *Environmental Science & Technology*, 35(18): 3620-3625.
74. Ion, A. C., Alpatova, A., Ion, I. and Culetu, A. (2011). Study on phenol adsorption from aqueous solutions on exfoliated graphitic nanoplatelets. *Materials Science and Engineering: B*, 176(7): 588-595.
75. Zakaa, A., Ibrahima, T. H., Khamisb, M. I. and Samarab, F. (2020). Adsorption characteristics of diclofenac sodium onto graphene nanoplatelets. *Desalination and Water Treatment*, 206: 331-339.
76. Al-Khateeb, L. A., Almotiry, S. and Salam, M. A. (2014). Adsorption of pharmaceutical pollutants onto graphene nanoplatelets. *Chemical Engineering Journal*, 248: 191-199.

77. Zakaa, A., Ibrahima, T. H., Khamisb, M. I. and Jabbara, N. A. (2019). Experimental design modelling and optimization of levofloxacin removal with graphene nanoplatelets using response surface method. *Pharmaceuticals*, 16(18): 19.
78. Kerkez-Kuyumcu, Ö., Bayazit, Ş. S. and Salam, M. A. (2016). Antibiotic amoxicillin removal from aqueous solution using magnetically modified graphene nanoplatelets. *Journal of Industrial and Engineering Chemistry*, 36: 198-205.
79. Banerjee, P., Das, P., Zaman, A. and Das, P. (2016). Application of graphene oxide nanoplatelets for adsorption of ibuprofen from aqueous solutions: evaluation of process kinetics and thermodynamics. *Process Safety and Environmental Protection*, 101: 45-53.
80. Rosli, F. A., Ahmad, H., Jumbri, K., Abdullah, A. H., Kamaruzaman, S. and Fathihah Abdullah, N. A. (2021). Efficient removal of pharmaceuticals from water using graphene nanoplatelets as adsorbent. *Royal Society Open Science*, 8(1): 201076.
81. ElHussein, E. A. A., Şahin, S. and Bayazit, Ş. S. (2020). Removal of carbamazepine using UiO-66 and UiO-66/graphene nanoplatelet composite. *Journal of Environmental Chemical Engineering*, 8(4): 103898.
82. Luo, X., Zhang, F., Ji, S., Yang, B. and Liang, X. (2014). Graphene nanoplatelets as a highly efficient solid-phase extraction sorbent for determination of phthalate esters in aqueous solution. *Talanta*, 120: 71-75.
83. Al-Khateeb, L. A., Hakami, W. and Salam, M. A. (2017). Removal of non-steroidal anti-inflammatory drugs from water using high surface area nanographene: kinetic and thermodynamic studies. *Journal of Molecular Liquids*, 241: 733-741.
84. Bhattacharya, S., Banerjee, P., Das, P., Bhowal, A., Majumder, S. K. and Ghosh, P. (2020). Removal of aqueous carbamazepine using graphene oxide nanoplatelets: Process modelling and optimization. *Sustainable Environment Research*, 30(1): 1-12.
85. Khalil, A. M., Memon, F. A., Tabish, T. A., Salmon, D., Zhang, S. and Butler, D. (2020). Nanostructured porous graphene for efficient removal of emerging contaminants (pharmaceuticals) from water. *Chemical Engineering Journal*, 398: 125440.